The role of mass-transport complexes (MTCs) in the initiation and evolution of submarine canyons

Nan Wu[1*], Harya D. Nugraha[2], Guangfa Zhong[1], Michael J. Steventon[3]

[1]State Key Laboratory of Marine Geology, Tongji University, Shanghai 200092, China

[2]Center for Sustainable Geoscience, Universitas Pertamina, Jakarta, 12220, Indonesia

[3]Shell Research, Shell Centre, London, SE1 7NA, UK.

*Email: nanwu@tongji.edu.cn

Abstract

The offshore area of the Otway Basin (SE Australia) is dominated by a multibranched canyon system where mass-transport complexes (MTCs) are widely distributed. Our study integrates high-resolution multibeam and seismic data to investigate the importance of MTCs in dictating the evolution of canyons. Our study interprets three regionally distributed MTCs that fail retrogressively and affect almost 70% of the study area. Within the MTCs, seven canyons that initiated from the continental shelf edge and extended to the lower slope are observed. Although the canyons share common regional tectonics and oceanography, the scales, morphology, and distribution are distinctly different. This is linked to the presence of failure-related scarps that control the initiation and formation of the canyons. The retrogressive failure mechanisms of MTCs have created a series of scarps on the continental shelf and slope regions. In the continental shelf, where terrestrial input is absent, the origin of the canyons is related to local failures and contour current activities, occurring near the pre-existing larger headwall scarps (c. 120 m high, 3km long). The occurrence of these local failures has provided the necessary sediment input for subsequent gravity-driven, downslope sediment flows. In the continental slope region, the widespread scarps can capture gravity flows initiated from the continental shelf, developing an area of flow convergence, which greatly widens and deepens the canyon system. The gradual diversion and convergence through MTC related scarps have facilitated the canyon confluence process, which has fundamentally changed the canyoning process. Thus, our study concludes that the retrogressive failure mechanism of MTCs has a direct influence on the initiation, distribution, and

evolution of the canyons. The scarps associated with MTCs have greatly facilitated the delivery of sediments and marine plastics from the shelf edge into the deep oceans, especially in areas where fluvial input is missing.

Keywords: Mass-transport complexes (MTCs); Submarine canyons; Otway Basin; South-east Australia

1. Introduction

Submarine canyons are defined as steep-sided V- or U-shaped valleys that erode into the seabed, they can extend from the continental shelf to the continental slope, with numerous tributaries (Shepard et al., 1966; Twichell and Roberts, 1982; Obelcz et al., 2014). Canyons are complex geomorphological features formed by erosion from gravity flows occurring near subaqueous slopes (Shepard, 1972; Canals et al., 2006; Harris and Whiteway, 2011). Canyons are often associated with sand-rich gravity flows which develop into submarine fans , which can act as high quality deepwater hydrocarbon reservoirs (Stow and Mayall, 2000; Weimer and Slatt, 2004; Steventon et al., 2021). Mass-transport complexes (MTCs) are gravity-driven shear failure deposits resulting from creep, spread, slide, slump and debris flow processes (Posamentier and Martinsen, 2011; Wu et al., 2021). MTCs can be extremely erosive, thus containing large volumes of sediments, with single deposits covering areas of >100 km^2 and volumes of >10,000 km^3 (Frey Martinez et al., 2005; Moscardelli and Wood, 2016; Nugraha et al., 2019). MTCs normally fail retrogressively (i.e. backstepping slope failures), and the emplacement of MTCs can leave a series of giant slide scars (c.2-5 km wide) on continental slope areas (Figure 1a, 1b; i.e. Williams, 2016; Li et al., 2017). Both MTCs and canyons can transfer large amounts of sediments between the continental shelf and abyssal plain environments, and are considered important sediment transportation processes in deepwater settings (McAdoo et al., 2000; Popescu et al., 2004; Antobreh and Krastel, 2006; Lee et al., 2007; Urgeles and Camerlenghi, 2013).

Submarine canyons and MTCs can have a close relationship in terms of their spatial distribution, triggering mechanisms, and preconditioning factors (Micallef et al., 2012; Watson et al., 2020). The emplacement of MTCs can represent the early phase of submarine canyon initiation, providing early depressions on the continental slopes that extend to the shelf break (Farre et al., 1983). The

continuous downcutting process associated with canyon development can steepen the gradient of canyon sidewalls, which preconditions the sidewalls to fail,depositing MTCs near the canyon walls (i.e. Farre et al., 1983; Green and Uken, 2008). These intra-canyon MTCs can occur retrogressively, increasing the canyon's width (i.e. lateral extension; Pratson and Ryan, 1994) and extending the canyon upslope (i.e. headward incision; Farre et al., 1983; He et al., 2014). However, most of the published works have focused on constraining local, coeval, intra-canyon MTCs (sensu detached MTCs; Moscardelli and Wood, 2008) with the evolution of canyons (i.e. Green and Uken, 2008; Gong et al., 2011; He et al., 2014; Su et al., 2020). The relationship between canyons with regional distributed MTCs (i.e. 100s to 100,000s of km^2) (senus attached MTCs; Moscardelli and Wood, 2008) that typically fails retrogressively have largely been overlooked. Relatively little is known on how regionally distributed MTCs, especially how their retrogressive failure mechanism can influence the initiation, evolution, and morphology of submarine canyons. Therefore, this study uses a high-resolution (c. 10 m vertical resolution) 3D seismic reflection dataset, integrated with 2D seismic and multibeam bathymetry data to analyse the spatial and temporal relations between canyons and regionally distributed MTCs in the Otway Basin, south-eastern Australia (Figure 2a, 2b).

2. Geological setting

2.1 Tectonic

The offshore Otway Basin is a broadly NW-SE striking non-volcanic rift basin, located along the south-eastern Australian passive margin (Figure 2b). The basin was initiated by late Jurassic to early Palaeogene rifting, during the progressive breakup of southern and eastern Gondwana. After experiencing multistage rifting, thermal subsidence and inversion, the south Australian margin ultimately broke-up with Antarctica at the end of the Cretaceous (approximately 67 Ma; Willcox and Stagg, 1990; Perincek and Cockshell, 1995; Krassay et al., 2004; Totterdell et al., 2014). Although the detailed history of the separation and final breakup between Australia and Antarctica remains partially studied (Gibson et al., 2013; Holford et al., 2014), the formation of a regionally distributed Maastrichtian unconformity has been attributed to the eventual separation of the Australian and Antarctica Plates (Figure 3a; Krassay et al., 2004; Holford et al., 2014).

2.2 Sedimentology

84 The Cenozoic sedimentary succession in the Otway Basin is composed of marine-related, often
85 calcareous-rich sediments, reflecting an open marine depositional environment (McGowran et al.,
86 2004). The Cenozoic post-rift sedimentation is represented by the Wangerrip Group (late
87 Palaeocene to middle Eocene, mainly siliciclastic rich), the Nirranda Group (middle Eocene to early
88 Oligocene, mainly containing sandstones and marls), the Heytesbury Group (late Oligocene to late
89 Miocene, mainly contains marls and limestones), and the Whalers Bluff Formation (WBF; Pliocene-
90 Recent, mainly contains mixed siliciclastic-carbonate sediment) (Figure 3a; Dickinson et al., 2002;
91 Krassay et al., 2004; Holford et al., 2014). Our study interval lies in the WBF formation at a time
92 when the study area was in a passive continental margin setting. In the continental slope area, a
93 thick, localised Pliocene-recent succession, represents marine clastic sediments deposited in and
94 around submarine canyons (Figure 3b, 3c) (Tassone et al., 2011).
95 *2.3 Oceanography*
96 Two shelf-break currents dominate ocean circulation in the study area (Duran et al., 2020): (i) the
97 eastward-flowing South Australia Current (SAC) and (ii) the south-eastward-flowing Zeehan Current
98 (ZC) (Figure 2b). The SAC is an eastward-flowing current with high salinity and velocity (0.5 m/s),
99 originating from the centre of the Great Australian Bight Basin (Rochford, 1986). The current
100 operates down to 200 m depth (Middleton and Bye, 2007). The ZC (fed by the South Australian
101 Current) is a poleward current with low salinity and high current velocity (0.4 m/s), flowing down
102 to 300 m water depth (Ridgway, 2007). The offshore area of the Otway Basin is also periodically
103 affected by seasonal cyclones and storms (Holland and Gray, 1983; Kuleshov et al., 2002). The
104 above-mentioned down-slope and along-slope marine oceanographic processes have jointly
105 influenced the oceanography and sedimentation in the Otway Basin.
106 As fluvial activity is limited in the study area (McGowran et al., 2004), the elongated mounded
107 seismic facies (sub-parallel to wavy, low- to high amplitude, internal truncations) in the WBF
108 Formation have a clear indication of contour current activity (Figure 3c). Similar seismic facies have
109 been interpreted as contourites that are affected by contourite currents in other submarine
110 settings (i.e. Stow and Faugères, 2008; Rebesco et al., 2014). Moreover, the modern canyons show
111 a clear eastward lateral migration compared to the buried Pliocene canyons in the continental shelf
112 region (Figure 3c). These observations all indicate that the overall eastward shelf-break parallel
113 currents (SAC and LC) affect the sedimentary processes in the continental shelf region.

3. Dataset and Methodology

3.1 Multibeam Dataset

The multibeam echosounder bathymetry data is provided by Geoscience Australia (https://portal.ga.gov.au/persona/marine), covering an area of c. 12,000 km^2 (Figure 4a). The lateral resolution of the data is 50 × 50 m, and it enables the identification and interpretation of seabed morphology and associated canyons and MTCs, especially in areas absent of seismic-reflection data (Figure 4a).

3.2 Seismic Dataset

The 3D pre-stack time migrated (PSTM) seismic-reflection data were acquired by Santos in 2002, located in the vicinity of Portland, offshore SE Australia (Figure 2b). The survey covers an area of c. 360 km^2 with a bin spacing of 25 m × 12.5 m (inline × crossline), and a dominant frequency of 50 Hz at the seabed. The study estimates that the spatial resolution of the seismic data, given an average velocity of the near seabed sediment derived from the seismic report (1824 m/s), is c. 9 m. The 3D seismic data are zero-phase, and presented in SEG normal polarity with an increase in acoustic impedance expressed as a positive amplitude.

3.3 Methodology

The seismic-stratigraphic framework is correlated with Holford et al. (2014) work in an adjacent area. Seismic and multibeam data are used to map MTC and canyon related features. The key morphometric parameters of the canyons (i.e. canyon width and height) are quantitatively measured and discussed to reveal the sedimentary processes involved in the canyon origin and evolution. In this study, the canyon width is defined as the distance between the canyon shoulders (the point at which the canyon margin begins to dip away from the canyon axis) (Figure 5; Laberg et al., 2000). The canyon height is defined as the depth from the canyon shoulder to the canyon base (Figure 5).

4. Result

4.1 Morphology of the seabed

The study area spans from the continental shelf to the continental lower slope environment (Figure

4a). The morphology of the study area is characterised as having a narrow (c. 7km) and steep slope (Figure 4b). The continental shelf area dips from 0.4° to 1° with an average water depth of 250 m (Figure 4b). The continental slope area is characterised by a relatively gentle slope of c. 10° in the upper section, to a steep slope gradient of c. 30° near the lower section, with water depths ranging from 600 m to 1500 m, respectively (Figure 4b). The multibeam reveals several canyons initiated from the continental shelf region, spanning the continental slope, and ultimately terminating in the abyssal plain (Figure 4a). Widely distributed MTCs and their associated headwall scarps and lateral margins have also been identified (Figure 4a). These MTCs have a close relationship with the canyons (Figure 4a). The topographic profiles extracted from the multibeam data in the abyssal plain show dramatic differences in the across-canyon margin morphology (Figure 4c). In the abyssal plain, where the seabed gradient is relatively low (<2°), the width and height of the canyons (i.e. Canyon-a and Canyon-b) increase along with the dip of the slope, with canyons converging at the deeper section of the abyssal plain (Figure 4c, 4d). The width of the canyon increases from c. 5.6-6.6 km to c. 10.9 km, and the height of the canyon increases from c. 300 m to 360 m, respectively (Figure 4c, 4d). The multibeam data used in this study can only investigate the seabed morphological features with a relatively limited lateral resolution (c. 50 by 50 m). It lacks the ability to examine the detailed seabed structures in 3D and reveal the characteristics of the buried sediments. Therefore, in the following section, this study uses high-resolution seismic reflection datasets to investigate the cause of the canyon converging process and the sedimentary process interactions between canyons and MTCs.

4.2 MTCs and canyons

Three MTCs (MTC-1, MTC-2, and MTC-3) have been interpreted in the study area (Figure 6a, 6b). Within these MTCs, the seismic reflection dataset reveals several distinctive E-trending scarps parallel to the slope strike direction and a set of SW-oriented lateral scarps parallel to the slope dip direction (Figure 6b). The arcuate E-dipping extensional scarps are interpreted as MTC headwall scarps that mark the updip part of an MTC, where extensional deformation dominates (Figure 6b; i.e. Bull et al., 2009). The SW-dipping lateral scarps are interpreted as MTCs lateral margins that separate deformed sediments (MTCs) from the undeformed seabed (Figure 6b; i.e. Frey Martinez et al., 2005; Bull et al., 2009). Based on the orientation of headwall scarps and lateral margins, the MTCs are predominately transported subparallel to the dip direction of the slope.

Seven major canyons (canyon 1-7) spanning from continental shelf to continental lower slope are observed within the MTC influenced area (Figure 6a, 6b). They are oriented NNW-SSE on the continental slope, sub-parallel to the slope dip direction, and the orientation changes to NNE-SSW in the lower slope setting (Figure 6a, 6b). Canyon-1-3 and Canyon-7 are initiated from shelf edge headwall scarps with clear landward incision features, while Canyon-4-6 are restricted in the continental slope (Figure 6b).

4.3 MTC-1

In MTC-1, multiple headwall scarps (HS-1 to HS-5; from older to younger) and their associated lateral margins are observed from map view and the correlated seismic sections (Figure 7a, 7b). Headwall scarps are recognised as upward concaved lineation with scallop-shaped geometries (Figure 7b). In the seismic dip section, the headwalls are nested in a terraced style, showing a truncated reflector that cuts through upslope sediments (Figure 8a). The heights and angles of the scarps vary considerably throughout MTC-1, with the highest (c. 170 m) and steepest (c. 40^{o}) HS-5 occurring in the upper part of MTC-1 (Figure 8a, 8b). The scale of the other four headwall scarps (HS-4 to HS-1) are comparatively smaller, and the gradient is gentler than HS-5. HS-1 to HS-4 show similar morphology to the HS-5, and they are distributed in the central part of the MTC-1 (Figure 7b, 8a-d). The middle part of MTC-1 has a hummocky seabed expression in map view and contains chaotic and blocky seismic facies in seismic section (Figure 7b, 8a). A clear basal shear surface with a gentle gradient (c. 3^{o}) separates the underlying layered seismic facies from the overlying chaotic seismic facies, observed below HS-5 and HS-1 (Figure 8a). The chaotic and blocky facies accumulated downdip of the HS-4 and HS-1, showing a wedge-shaped geometry in seismic section (Figure 8a) and a fan-shaped geometry in plain view (Figure 7b).

The presence of the backstepping stair shape geometry, the relative flat basal shear surface, and the deposition of chaotic seismic facies near the distal part of HS-4, HS-3, and HS-2, suggests that the initial failure started at the lowermost part of MTC-1 and propagated retrogressively towards the upper slope area. Our study thus interprets multiple headwall scarps (HS-1 - HS-5) resulting from multiple retrogressive failure events, such as recorded in the Storegga slide and other well studied MTCs (i.e. Bryn et al., 2005; Sawyer et al., 2009; Badhani et al., 2020). The occurrence of retrogressive failure has resulted in linear to sinuous depression features in plan-view (Figure 7b), and small-scale faults or fractures in seismic cross-sections (see headwall scarps in Figure 8b-d).

4.4 Canyons in MTC-1

In the upper section of MTC-1, the canyon system comprises three tributaries (Canyon-1 to Canyon-3; Figure 6b, 7b), which terminate to the scarps near the shelf edge (Figure 6b). Canyon-1 and -2 are developed in the NE part of MTC-1, while Canyon-3 is in the NW part (Figure 7b). Canyon 1-3 have more pronounced seabed erosion than MTC-1. Near HS-5, clear seabed incision and truncations can be observed in the seismic sections that image the canyons (Figure 8a, 8b). Canyons 1-3 have a linear geometry in map view. The cross-sectional geometry of the canyons is generally U-shaped, with a gently sloping base surface (c. 1^{o}) and steep canyon sidewalls (c. 60^{o}) (Figure 8b, 8c). Canyons 1-3 trend downslope from the continental shelf towards HS-5 and converge near HS-3 (the confluence point; Figure 7b, 7c), and ultimately converging into a broad canyon after passing through HS-2, at a water depth 1522 m to 1595 m (Figure 7b, 7c, 8d). Numerous crescentic bedforms and axial incisions are observed along the axis of Canyon 1-3 (Figure 7b, 7c). In the pre-confluence region, the Canyons 1-3 range from c. 100 m to c. 670 m wide and c. 20 m to 134 m high (Figure 9a, 9b). In the post-confluence area, the width increases from c.370 m to c.1140 m, which is 2-3 times wider than that of in the pre-confluence region (Figure 9a). The canyon height increases from c. 90 m to c. 140 m in the post-confluence area, slightly larger than the canyons in the pre-confluence area (Figure 9b).

This stratigraphic relationship between canyons and MTC-1 indicate that the deposition of the MTC-1 occurred prior to the initiation of canyons. The crescentic bedforms are possibly associated with supercritical currents (i.e. Zhong et al., 2015), suggesting gravity flows are still being initiated, and canyons are remaining active as a sediment pathway today. Quantitative analyses of the canyons indicate a strong correlation exists between the canyon width/height with distance along the different MTC-1 headwall scarps. The increase of the canyon's width and depth after the confluence point (near the HS-2) indicate headwall scarps have played a key role in dictating the canyon morphology and incision depth. The abrupt increase in canyon width after the confluence can be interpreted as an increase in discharge, because the converged canyon can be subjected to gravity flows from multi-sources (see the similar process from Mitchell, 2004). Our study thus indicates the topography within MTC-1 was established as a function of topographic confinement imposed by the backstep headwall scarps. The existence of the headwall scarps can facilitate the canyon widening and deepening process.

4.5 MTC-2 and MTC-3

MTC-2 was deposited at the west of the MTC-1 (Figure 6b), it contains four internal headwall scarps (HS-1 to HS-4; from older to younger) and associated lateral margins (Figure 10a, 10b). Along the proximal part of the western lateral margin, the sidewall displays up to at least three levels of local retrogressive failures that make the west lateral margin complex (Figure 10b). The cross-cutting relationship between MTC-1 and MTC-2 reveals MTC-2 occurred after MTC-1. Similar to MTC-1, the multi-headwall scarps are the result of retrogressive failure events associated with the emplacement of MTC-2. MTC-3 was deposited in the west of the study area (Figure 6b). Distinctive NNW-ESE dipping headwall scarps can be only identified near the upper boundary of MTC-3 (Figure 10b). The number of scarps in MTC-3 are significantly less than those in the MTC-1 and MTC-2 (Figure 10b).

4.6 Canyons in MTC-2

Two canyons (Canyon-4 and Canyon-5) that initiated from the lower slope setting, were observed and incised across MTC-2, with a small (c. <50 m height) bathymetric expression in plan view (Figure 10a, 10b). Upslope from the Canyon-4 head, a channel is observed from map view (Figure 10b). The morphology of Canyon-4 is only visible in map view near the lower slope, and it loses surface expression at the location of HS-4 (Figure 10b). Upslope from the Canyon-5 head, two channels are observed from map view (Figure 10b). The morphology of Canyon-5 meanders around the headwall scarps within MTC-2, being initially WNW-SE strike at the location of HS-4 and HS-3, shifting to SE at the site of HS-2, and shifting again to an abrupt SW bend at HS-1 (Figure 10b). After passing through HS-1, Canyon-5 is oriented southward (Figure 10b). Seismic profiles of canyon-5 reveal a U-shaped erosional feature, and the cross-sectional morphology keeps constant along the canyon-5's pathway (Figure 11a-c). The width and height of canyon-5 varies compared to Canyon-1 (Figure 11d). The upper reach of canyon-5 has a deeper incision and width that can reach 76 m and 565 m, respectively. In the lower slope, the width of canyon-5 decreases from 565 m to c. 370 m and increases to 750 m after passing through HS-3 (Figure 11d). The width of Canyon-5 drops sharply to 343 m after passing through HS-1. The height of the Canyon-5 constantly decreases from c. 58 m near the HS-4 to c. 44 m near the HS-1 (Figure 11d). In summary, from the HS-4 to HS-1, Canyon-5 becomes narrower and less incised.

Limited distribution of Canyon-4 indicates that the canyon incision has been isolated to the lower

slope. The rapid shifting of the Canyon-5 pathway orientations indicates that the presence of headwall scarps can influence and divert canyon transport direction. Canyon-5 has a clear backstep (landward) incision and connects with the shelf edge headwall scarp by channels, and this might suggest Canyon-5 is still active during the Holocene. Our study suggests with the headward incision associated with canyon-5, once the canyon head connects to shelf edge headwall scarps, it will develop into a 'mature' stage akin to the canyons in MTC-1.

4.7 Canyons in MTC-3

Two canyons (Canyon-6 and Canyon-7) are observed in MTC-3 (Figure 10b). The morphology of Canyon-6 is only visible close to the lower slope (Figure 10b). Further downslope, Canyon-6 lose its morphology in map view, and there is no visible canyon form in the seismic section (Figure 12b, 12c). Canyon-7 has a tripartite, concave head that cuts c.7 km landward into the shelf (Figure 10b). The cross-sectional geometry of Canyon-7 shows a clear V-shaped incision (Figure 12a, 12b). However, this V-shaped downcutting geometry is only constrained in the lower slope region. The width and height of Canyon-7 are low in the lower slope setting, ranging from c. 120 m to 175 m and c. 20 m to 50 m, respectively (Figure 12d).

Canyon-6 and Canyon-7 have a broad flat canyon floor, with less signs of incised channels. The flat canyon floor might indicate that the gravity flow contributes to the formation of canyons have been largely displaced due to the absence of headwall scarps. Moreover, due to the absence of the scarps, Canyon-6 and Canyon-7 show a low sinuosity and a subparallel pathway. No major canyon diverting nor converging has been observed in the MTC-3 region (Figure 10b).

5. Discussion

5.1 Origin of the canyons

Based on the morphology and depositional process, submarine canyons can be classified into two main types (Type I and Type II from Jobe et al., 2011). Type I canyons normally indent the shelf edge and are linked with a clear bathymetric connection to fluvial systems. These canyons can receive abundant coarse-grained sediment supply and generate erosive canyon morphologies (Jobe et al., 2011). Type II canyons normally indent the continental slopes, and they don't have a clear bathymetric connection to fluvial systems (thus a low sediment supply). Therefore, the Type

II canyons normally exhibit smooth and aggradational morphologies (Jobe et al., 2011). In this study, the study area is disconnected from the modern fluvial system (Leach and Wallace, 2001), which indicates a limited sediment input at or near the canyon heads. The canyons are thus sediment starved when compared to canyons connected with direct fluvial input (e.g. the Type I canyons) or canyons which are in close proximity to high supplies of coarse-grained sediment (Smith et al., 2018). Similar canyons (e.g. the Type II canyons) that are isolated from major river input, with linear morphology of low sinuosity, have been documented from other margins (e.g. Harris and Whiteway, 2011; Jobe et al., 2011). The initiation of the Type II canyons are connected to local failures near continental margins or slopes, which is independent of sediment input (i.e. river feed) and sea-level fluctuation (Normandeau et al., 2014). Other triggers, such as mixed constructions and modification by turbidity and contour currents near the canyon heads have also been suggested as potentially initiation machanisms for Type II canyons (i.e. Jobe et al., 2011). This has also been inferred for canyons in the South China Sea (Zhu et al., 2010), and other submarine localities (i.e. Rebesco et al., 2007). In this study, the morphology of the canyon heads is strictly constrained within the headwall scarps near the shelf edge (Figure 13a, 13b). The spatial relation between the shelf edge headwall scarps and canyon heads suggests the initiation of canyons is closely related to these pre-existing, steep shelf edge headwall scarps (Figure 13a, 13b). Moreover, as the contour current is active near the shelf edge area, the movement of the contour current along the topographically low scarps may induce local turbulence and produce down-canyon sediment transportation (i.e. Fenner et al., 1971; Warratz et al., 2019). Thus, our study suggests that the canyon systems in the study area are initiated by a combination of multistage retrogressive failure events and contour current activity near the pre-existing headwall scarps at the continental shelf edge (Figure 13c). Although the study area lacks river-sourced sediments, canyon heads can still capture sediments from local failures associated with the contour current activities. These local failures and the associated gravity flows can erode the seabed and facilitate canyon development from upper slope to lower slope (Figure 13d) (see also similar process from Atlantic canyons; Twichell and Roberts, 1982). Other factors, such as cyclones (hurricane or typhoon) and tidal currents occurring in the continental shelf area, may also contribute to canyon initiation (Shepard et al., 1974; Sequeiros et al., 2019). Hurricanes and typhoons can trigger waves and currents, thus resuspending and carrying sediment. These processes will directly play a role in initiating turbidity

currents, which bring sediments into the canyon heads and enhance the canyoning process (Sequeiros et al., 2019). Tidal currents can act as an efficient force for reworking and carrying sediments in submarine settings (Shepard et al., 1974). Tidal currents can thus transport sediments into the canyon heads, especially at places where fluvial input is missing.

5.2 Role of retrogressive failure mechanism on canyon evolution

The headwall scarps of MTCs play an essential role in capturing turbidity currents and facilitating turbidity channelization in submarine settings, as demonstrated by examples from previous seismic- and outcrop-based studies (Loncke et al., 2009; Alves and Cartwright, 2010; Ito, 2013; Qin et al., 2017; Li et al., 2020). The three MTCs presented in this study have indicated the spatial variation of canyon morphology is linked with the MTCs morphometric characteristics. This study further splits these MTCs into two types based on their morphology (Type-1 and Type-2; Table 1). Type-1 MTCs (e.g. MTC-1 and MTC-2) are characterised as having multiple internal headwall scarps, and Type-2 MTCs (e.g. MTC-3) are characterised with no visible internal headwall scarps. In the following section, our study attempts to define the possible mechanisms influencing different types of MTCs and their impact on canyon evolution.

For Type-1 MTCs, the retrogressive failure events associated with MTC-1 have left a pronounced negative seabed space that greatly changed the slope morphology and created a series of localised seabed 'ponding' accommodation spaces along the pathway of submarine canyon systems. The gravity-driven downslope processes are sensitive to the slope gradient variations, preferentially depositing where the gradient decreases the most (Kneller et al., 2016). The varied hierarchies of headwall scarps can therefore trap or divert subsequent turbidity currents and facilitate canyon systems' incision and development. Though the headwall scarps within MTC-2 does not widen nor deepen canyons that are transported through, they do play an essential role in changing the canyon direction. Type-2 MTCs have less influence on the canyoning process, providing a differing example of how headwall scarps can influence canyon evolution. MTC-3 demonstrates that an absence of internal headwall scarps, produces a lack of ability to trap or capture the turbidity currents that flow through. Though Canyon-7 has connections to the shelf edge headwall scarps, the scale of the canyon is smaller than those in the other two MTCs (i.e. Canyon-3 in MTC-1; Figure 6a, 6b). Therefore, our study indicates that the retrogressive failure mechanism of MTCs is responsible for the canyon deepening and confluence process, which can greatly influence the canyons'

morphology.

5.3 Other factors that may influence the evolution of the canyon

The evolution of submarine canyons can also be influenced by many other geological factors, including (i) regional tectonics (i.e. regionally distributed faults), which influence the sediments strength, thus the susceptibility to erosion during the formation of canyons (Covault et al., 2007); (ii) the sea-level variation, which can vary sediment input into canyon heads (Vail, 1977; Posamentier et al., 1991); (iii) downslope and along-slope depositional processes (i.e. gravity flows and contour currents), which erode the seabed and enlarge submarine canyons (Pratson and Coakley, 1996; He et al., 2014; Miramontes et al., 2020).

In this study, tectonics is unlikely to be of significance for canyon development due to the relatively stable nature of the southern Australian passive margin. Sediments in such a stable setting typically exhibit lower shear strength as compared to their active margin counterparts (Sawyer and DeVore, 2015; DeVore and Sawyer, 2016). In active margins, the higher sediments shear strength is interpreted to be due to the repeated exposure to earthquake energy that gradually increases shear strength by shear-induced compaction and dewatering processes (i.e. seismic strengthening, *sensu* Sawyer and DeVore, 2015). Therefore, the absence of intense tectonics and seismicity may thus have a significant role in preconditioning slope failures in passive margins, resulting to widely distributed MTCs (i.e. Sawyer and DeVore, 2015; DeVore and Sawyer, 2016). Recent studies revealed that the canyon initiation process does not necessarily depend on sea-level rise and fall, as well-developed canyon systems have been identified during highstands in many submarine settings (i.e. Xu et al., 2010; Paull et al., 2013; Normandeau et al., 2015). In the study area, the modern canyons are contiguous with Pliocene canyon systems, showing similar geometries and slightly eastward migrated distribution patterns. The similarities between buried Pliocene and modern canyons indicate that the location and distribution of modern canyons are an extension of the infilled Pliocene canyon systems. The overall eastward canyon lateral migration during Pliocene-Recent is interpreted to be related to theeastward shelf break parallel paleocurrent (i.e. SAC or LC), which is still active near the current-day shelf edge (Godfrey et al., 1986). Moreover, our study suggests that the types of the underlying deposits can also influence the morphology of the canyons. For example, Canyon-1 to Canyon-3 deposit above the slope background deposits (Figure 8b), while Canyon-6 deposits above a buried MTC (Figure 12c). The quantitative analyses

reveal that the scale of the Canyon-1 to Canyon-3 (immediately above background deposits) is larger than that of the Canyon-6 (immediately above buried MTCs). The scale contrast is interpreted due to buried MTCs, which are typically more consolidated than undeformed background slope deposits (i.e. Shipp, 2004; Sawyer, 2007; Wu et al., 2021). Thus, the incision depth and scale of Canyon-6 is smaller than other canyons.

5.4 Canyon evolution model

Our study attempts to build an updated model of canyon formation based on the models proposed by Pratson and Coakley (1996) and Jobe et al. (2011), emphasising the role of headwall scarps associated with regionally distributed MTCs. Our model consists of three phases, the occurrence of retrogressive failures, the initiation stage of the canyons, and the canyon transition stage.

Phase 1: the occurrence of the retrogressive failures

Prevailing eastward-flowing contour currents continuously deposit sediment near the shelf edge (Figure 14a). Seismicity (i.e. Bornhold and Prior, 1989), sediment overloading generated overpressure (i.e. Dugan and Flemings, 2000), or tectonic oversteepening (i.e. Moscardelli et al., 2006), or other triggering mechanisms (ADD REFERENCE) activated the initial failures in the lower slope setting (Figure 14a). The initial failure creates an open scarp, that leaves the sediments in the up-dip area unstable. As the gravitational strain accumulates, the sediments near the initial scarp weaken. A new extensional failure (the second scarp) will occur behind the initial scarp once the sediments become weaker than the along slope gravity-induced stress (Figure 14a). The failure process will continue up-dip until final balance has been achieved between the shear strength of the slope sediments and the shear stress of the gravitational forces (Figure 14b, 14c; Sawyer et al., 2009). This retrogressive failure mechanism has left a series of headwall scarps and lateral scarps on the continental shelf and slope (Figure 14c). The scarp-rich environment represents the preliminary phase of canyon initiation.

Phase 2: the initial stage of the canyon system

The erosional processes near the headwall scarps have led to triangular-shaped canyon heads (Figure 14d). The failed sediments associated with erosional processes near the shelf edge could excavate the pre-existing headwall scarps and contribute to the initial sediment influx for canyon initiation (see the similar process from Pratson and Coakley, 1996; Puga-Bernabéu et al., 2011). There are other erosional processes that could also account for the initial sediment influx, and

409 therefore may have also contributed to canyon initiation. Firstly, sediments collapsed from the
410 canyon sidewalls (canyon flank failures) can form downslope-flowing turbidity currents, facilitating
411 the canyon flushing process. The failure events associated with the pre-existing headwall scarps
412 and canyon sidewalls allow the delivery of sediment enabling canyon formation and downward
413 incision (Pratson and Ryan, 1994; Pratson and Coakley, 1996; Armitage et al., 2010). Secondly,
414 contourites may fail periodically, due to the seasonal cyclone (hurricane or typhoon) activities, or
415 sediments overpressure generated by rapid deposition of fine-grained sediments (Sequeiros et al.,
416 2019; Brackenridge et al., 2020; Gatter et al., 2020). The periodical failure processes can create
417 local turbulence near the shelf edge headwall scarps, which further facilitate the formation of flows
418 that carry sediments into the canyon heads (Figure 14d).
419 *Phase 3: the canyon transitional stage*
420 With the continuous failures near the shelf edge headwall scarps, the canyon heads gradually
421 establish into triangular or dendritic shapes. These triangular or dendritic shape structures
422 facilitate canyon head capture and funnel larger volumes of sediments into the canyon, and the
423 canyoning process becomes self-propagating (Figure 14d). The failed sediments near the headwall
424 scarps in the continental shelf converged into the channel-shaped conduit, acting as catchment
425 areas for sediments. Downward sediment gravity flows generated by the failed sediments can
426 contribute significantly to the ongoing canyon excavation and downslope propagation (Popescu et
427 al., 2004; Baztan et al., 2005). The presence of the headwall scarps on the slope provide further
428 sediment input and canyon tributary convergence (Figure 14d). The canyons are thus progressively
429 propagating to the lower slope and abyssal plain.
430 *5.5 Implication*
431 Many studies have shown how submarine MTCs rugose top surface can capture/reroute
432 subsequent sediment pathways based on seismic data (Loncke et al., 2009; Ortiz-Karpf et al., 2015;
433 Qin et al., 2017) and outcrops (Armitage et al., 2009; Jackson and Johnson, 2009; Kneller et al.,
434 2016). These studies are examples of MTCs located near the shelf edge where the sediment supply
435 is high. The rugose top surfaces developed along the upper surface of MTCs is caused by the
436 cohesive nature of the failures, along with the presence of internal structures such as megaclasts,
437 fold-thrust systems, and pressure ridges (see Bell et al 2009, Steventon et al 2019). The rugose
438 topography can be healed quickly by subsequent sand-rich turbidity currents or separate failures.

Thus, MTCs have a direct influence on the location and distribution of reservoirs and important implications for hydrocarbon exploration.

Conversely, our study documents MTCs in low sediment supply margins where large-scale sediment bypass is missing. Our study shows strong evidence that the emplace of MTCs has played a key role in influencing the evolution of canyon systems. Our study develops a generic model of the MTCs headwall scarps, as a function of triggering and influencing the morphological evolution of canyons, thus controlling the sediment bypass from the shelf edge to lower slope and abyssal plain. Our study indicates that retrogressive failure mechanism can facilitate long-distance sediment transportation within canyon systems, and may be a common process in a submarine setting where modern river systems are absent.

Previous studies have revealed that the density of marine plastics in canyons are 2-3 times larger than the adjacent slopes or shelves (Pham et al., 2014; Cau et al., 2017; Kane et al., 2020). The plastic pollutants can be transported across the shelf by contour currents and delivered to submarine canyon heads formed far from terrestrial input (i.e. 150 km away from the coastline; Zhong and Peng, 2021). Therefore, canyons not only can act as a major conduit for delivering sediments, but they can also receive and transport marine plastics from shallow marine environments into the deep ocean (Kane et al., 2020).

In this study, the canyon heads are subjected to episodic turbidity currents. Therefore they can receive sediments and plastics delivered by contour currents near the shelf edge (i.e. Kane et al., 2020; Zhong and Peng, 2021). Moreover, as the MTCs can facilitate longer transport distance of sediments and plastics within canyons into the deep ocean, plastics delivered by canyon systems may thus have the ability to travel into the deep Southern Ocean, with associated environmental impacts (Zhong and Peng, 2021). Therefore, a combination of a high-resolution bathymetry dataset with manned submersible dives is needed to further study this subject. The high-resolution bathymetry dataset can provide detailed imaging of the seabed and better constrain the role of MTCs during the canyon evolution. The manned submersible dives can establish plastic and/or microplastic density in the deeper marine region, which will help to understand and mitigate against anthropogenic impacts on the marine environment.

6. Conclusion

This study uses multibeam bathymetry and seismic reflection data to document how the retrogressive failure mechanism of MTCs has influenced the origin, geometry, and distribution of canyons in sediment starved submarine settings. In summary: (i) the emplacement of MTCs have left multi-scaled headwall scarps and lateral margins on the continental margin and slope area, (ii) the local failures developed associated headwall scarps near the continental shelf-edge have provided the initial sediment supply for canyon evolution, (iii) the headwall scarps which developed in the slope setting may act as the preferential pathways for sediment gravity flows, and facilitate canyon development, (iv) our study thus indicates that retrogressive failure mechanism can facilitate long-distance sediment transportation within canyon systems in starved submarine settings.

Data Availability

The seismic reflection data (OS02 3D survey and OS02 2D survey) and bathymetric data used in this study can be requested from the Geoscience Australia Repository https://www.ga.gov.au/data-pubs. The GEBCO_2014 bathymetry map can be downloaded from the Gridded Bathymetry Data Repository https://www.ngdc.noaa.gov/maps/autogrid/.

Figure Captions

Figure 1. (a) Model showing the time evolution of retrogressively failed MTCs, modified from Sawyer et al. (2009). (b) Schematic sketch showing the different stages of a retrogressive failure, modified from Locat et al. (2011).

Figure 2. (a) Regional map of the study area. (b) Zoom-in view of the study area showing the location of the city Portland and the Otway Basin. The white lines represent 2D seismic reflection data, and the red polygon represents the location of the 3D seismic reflection dataset. Shaded relief GEBCO_2014 bathymetry map downloaded from https://www.ngdc.noaa.gov/maps/autogrid/. Abbreviations for the Otway Basin are as follows:

492 SAC: South Australia Current, ZC: Zeehan Current.

493 Figure 3. (a) Stratigraphic and basin event chart for the Otway Basin (modified after Krassay et al.,
494 2004), including lithology interpretation and major tectonic events. The Horizon H1 has been
495 correlated to the intra-Maastrichtian unconformity surface from Holford et al. (2014). The Horizon
496 H2 is correlated to the base of the WBF. (b) Regional along slope seismic-section showing the
497 overall tectonic of the study area. See location from Figure 2b. (c) Regional seismic section that is
498 perpendicular to the slope, showing the key seismic horizons (H1 to the seabed) and canyon
499 bearing intervals. See location from Figure 2b.

500 Figure 4. (a) Multibeam bathymetry map of the study area illustrating the seabed morphology. The
501 red polygon stands for the location of 3D seismic data. The location of this figure is marked by the
502 black dashed line in Figure 2b. (b) Bathymetric profile along the slope direction, showing the
503 seabed morphology of the continental shelf, the continental slope and the abyssal plain. (c)
504 Bathymetric profile crossing the abyssal plain, showing the cross-sectional morphology of two
505 canyon systems (Canyon-a and Canyon-b). (d) Bathymetric profile revealing the combination of the
506 two canyon systems. See location in Figure 4a.

507 Figure 5. Schematic diagram showing the morphological parameters used in the quantitative
508 analyses of the canyons, including the width and height. (a) Uninterpreted cross-section of the
509 canyon system. (b) Interpreted cross-section of the canyon system with parameters used in
510 quantitative analyses.

511 Figure 6. (a) Contoured seabed map of the study area extracted from the 3D seismic reflection data.
512 (b) Schematic representation of seabed geomorphologic interpreted from Figure 6a. See the
513 location of this figure from Figure 2b.

514 Figure 7. (a) Zoomed in contoured seabed map showing the region of MTC-1. (b) Interpreted map
515 of Figure 7a, showing the major headwall scarps in MTC-1 and the location of Canyon-1, Canyon-2,
516 and Canyon-3. (c) 3D view of the canyon confluence geometry in MTC-1, and the crescentic
517 bedforms within canyons. See the location of Figure 7c in Figure 7b.

518 Figure 8. (a) The N-S oriented seismic section of MTC-1 shows backstep shaped headwall scarps
519 and MTC-1's basal shear surface. (b) Seismic cross-section cutting through HS-5 and HS-4, showing
520 the cross-section of the upper part of the Canyon-1, Canyon-2, and Canyon-3. (c) Seismic cross-
521 section cutting through HS-3, showing the cross-section of the proximal part of the Canyon-1,

Canyon-2, and Canyon-3. (d) Seismic cross-section cutting through HS-2 and HS-1, showing the cross-section of the post confluence part of the canyon system in MTC-1. See the location of Figure 8a-d in Figure 7a.

Figure 9. (a) Width profile of the canyon system in MTC-1. (b) Height profile of the canyon system in MTC-1.

Figure 10. (a) Zoomed in contoured seabed map showing the location of MTC-2 and MTC-3. B) Interpreted map of Figure 10a, showing the headwall scarps in MTC-2 and MTC-3, and the location of Canyon-4, Canyon-5, Canyon-6, and Canyon-7.

Figure 11. (a) Seismic cross-section cutting through HS-5 and HS-4 of MTC-2, showing the upper part of the Canyon-4 and Canyon-5. (b) Seismic cross-section cutting through HS-2 of MTC-2, showing the proximal part of the Canyon-5. (c) Seismic cross-section cutting through MTC-2, showing the distal part of Canyon-5. See the location of Figure 11a-c in Figure 10a. (d) Width and height profile of the Canyon-5 in MTC-2.

Figure 12. (a) Seismic cross-section cutting through the headwall of MTC-3, showing the upper part of the Canyon-7. (b) Seismic cross-section showing the proximal part of the Canyon-6 and Canyon-7. (c) Seismic cross-section showing the distal part of Canyon-6 and Canyon-7. See the location of Figure 12a-c in Figure 10a. (d) Width and height profile of the Canyon-7 in MTC-3.

Figure 13. (a) 3D view of seabed morphology showing the head of Canyon-5 and Canyon-7, and the headwall scarps occurring on the shelf edge. See location in Figure 5a. (b) 3D view of seabed morphology showing the head of Canyon-3, and the headwall scarps occurring on the shelf edge. See the location of Figure 13a-b in Figure 6a. (c) Sketch of 2D view of seabed morphology showing the headwall collapse and the initial stage of canyon evolution on the shelf edge. (d) Sketch of 2D view of seabed morphology showing the formation of the canyons.

Figure 14. Schematic figure showing the evolution model of the canyon system in the study area. (b) The schematic figure shows that the initial failure was created in the lower slope area, and a series of headwall scarps occurred updip of the initial failure. (b) The schematic figure shows the deposition of contourite drifts near the shelf edge, and the occurrence of slope attached MTCs near the lower slope. (c) The schematic figure shows the retrogressively failed MTCs and widely distributed headwall scarps in the continental shelf and slope settings. (d) The schematic figure shows that canyons were captured, converged and re-directed by the pre-existing headwall scarps.

Table Caption

Table 1. Classifications of MTCs and their influence on the canyon evolution.

Reference

Alves, T.M., Cartwright, J.A., 2010. The effect of mass-transport deposits on the younger slope morphology, offshore Brazil. Marine and Petroleum Geology 27, 2027-2036.

Antobreh, A.A., Krastel, S., 2006. Morphology, seismic characteristics and development of Cap Timiris Canyon, offshore Mauritania: a newly discovered canyon preserved-off a major arid climatic region. Marine and Petroleum Geology 23, 37-59.

Armitage, D.A., Piper, D.J., Mcgee, D.T., Morris, W.R., 2010. Turbidite deposition on the glacially influenced, canyon-dominated Southwest Grand Banks Slope, Canada. Sedimentology 57, 1387-1408.

Armitage, D.A., Romans, B.W., Covault, J.A., Graham, S.A., 2009. The influence of mass-transport-deposit surface topography on the evolution of turbidite architecture: the Sierra Contreras, Tres Pasos formation (Cretaceous), southern Chile. Journal of Sedimentary Research 79, 287-301.

Badhani, S., Cattaneo, A., Dennielou, B., Leroux, E., Colin, F., Thomas, Y., Jouet, G., Rabineau, M., Droz, L., 2020. Morphology of retrogressive failures in the Eastern Rhone interfluve during the last glacial maximum (Gulf of Lions, Western Mediterranean). Geomorphology 351, 106894.

Baztan, J., Berné, S., Olivet, J.-L., Rabineau, M., Aslanian, D., Gaudin, M., Réhault, J.-P., Canals, M., 2005. Axial incision: The key to understand submarine canyon evolution (in the western Gulf of Lion). Marine and Petroleum Geology 22, 805-826.

Bornhold, B.D., Prior, D.B., 1989. Sediment blocks on the sea floor in British Columbia fjords. Geo-Marine Letters 9, 135.

Brackenridge, R.E., Nicholson, U., Sapiie, B., Stow, D., Tappin, D.R., 2020. Indonesian Throughflow as a preconditioning mechanism for submarine landslides in the Makassar Strait. Geological Society, London, Special Publications 500, 195-217.

Bryn, P., Berg, K., Forsberg, C.F., Solheim, A., Kvalstad, T.J., 2005. Explaining the Storegga slide. Marine and Petroleum Geology 22, 11-19.

Bull, S., Cartwright, J., Huuse, M., 2009. A review of kinematic indicators from mass-transport complexes using 3D seismic data. Marine and Petroleum Geology 26, 1132-1151.

Canals, M., Puig, P., de Madron, X.D., Heussner, S., Palanques, A., Fabres, J., 2006. Flushing submarine canyons. Nature 444, 354-357.

Cau, A., Alvito, A., Moccia, D., Canese, S., Pusceddu, A., Rita, C., Angiolillo, M., Follesa, M.C., 2017. Submarine canyons along the upper Sardinian slope (Central Western Mediterranean) as repositories for derelict fishing gears. Marine pollution bulletin 123, 357-364.

Covault, J.A., Normark, W.R., Romans, B.W., Graham, S.A., 2007. Highstand fans in the California borderland: The overlooked deep-water depositional systems. Geology 35, 783-786.

DeVore, J.R., Sawyer, D.E., 2016. Shear strength of siliciclastic sediments from passive and active margins (0–100 m below seafloor): insights into seismic strengthening, Submarine Mass Movements and their Consequences. Springer, pp. 173-180.

Dickinson, J.A., Wallace, M.W., Holdgate, G.R., Gallagher, S.J., Thomas, L., 2002. Origin and timing of the Miocene-Pliocene unconformity in southeast Australia. Journal of Sedimentary Research 72, 288-303.

Dugan, B., Flemings, P.B., 2000. Overpressure and fluid flow in the New Jersey continental slope: Implications for slope failure and cold seeps. Science 289, 288-291.

Duran, E.R., Phillips, H.E., Furue, R., Spence, P., Bindoff, N.L., 2020. Southern Australia Current System

based on a gridded hydrography and a high-resolution model. Progress in Oceanography 181, 102254.
Farre, J.A., McGregor, B.A., Ryan, W.B., Robb, J.M., 1983. Breaching the shelfbreak: passage from youthful to mature phase in submarine canyon evolution.
Fenner, P., Kelling, G., Stanley, D.J., 1971. Bottom currents in Wilmington submarine canyon. Nature Physical Science 229, 52-54.
Frey Martinez, J., Cartwright, J., Hall, B., 2005. 3D seismic interpretation of slump complexes: examples from the continental margin of Israel. Basin Research 17, 83-108.
Gatter, R., Clare, M.A., Hunt, J.E., Watts, M., Madhusudhan, B., Talling, P.J., Huhn, K., 2020. A multi-disciplinary investigation of the AFEN Slide: the relationship between contourites and submarine landslides. Geological Society, London, Special Publications 500, 173-193.
Gibson, G.M., Totterdell, J., White, L.T., Mitchell, C., Stacey, A., Morse, M., Whitaker, A., 2013. Pre-existing basement structure and its influence on continental rifting and fracture zone development along Australia's southern rifted margin. Journal of the Geological Society 170, 365-377.
Godfrey, J., Vaudrey, D., Hahn, S., 1986. Observations of the shelf-edge current south of Australia, winter 1982. Journal of Physical Oceanography 16, 668-679.
Gong, C., Wang, Y., Zhu, W., Li, W., Xu, Q., Zhang, J., 2011. The Central Submarine Canyon in the Qiongdongnan Basin, northwestern South China Sea: architecture, sequence stratigraphy, and depositional processes. Marine and petroleum Geology 28, 1690-1702.
Green, A., Uken, R., 2008. Submarine landsliding and canyon evolution on the northern KwaZulu-Natal continental shelf, South Africa, SW Indian Ocean. Marine Geology 254, 152-170.
Harris, P.T., Whiteway, T., 2011. Global distribution of large submarine canyons: Geomorphic differences between active and passive continental margins. Marine Geology 285, 69-86.
He, Y., Zhong, G., Wang, L., Kuang, Z., 2014. Characteristics and occurrence of submarine canyon-associated landslides in the middle of the northern continental slope, South China Sea. Marine and Petroleum Geology 57, 546-560.
Holford, S.P., Tuitt, A.K., Hillis, R.R., Green, P.F., Stoker, M.S., Duddy, I.R., Sandiford, M., Tassone, D.R., 2014. Cenozoic deformation in the Otway Basin, southern Australian margin: Implications for the origin and nature of post‐breakup compression at rifted margins. Basin Research 26, 10-37.
Holland, G.J., Gray, W.M., 1983. Tropical cyclones in the Australian/southwest Pacific region. Colorado State University. Libraries.
Ito, M., 2013. The role of slump scars in slope channel initiation: a case study from the Miocene Jatiluhur Formation in the Bogor Trough, West Java. Journal of Asian Earth Sciences 73, 68-86.
Jackson, C.A., Johnson, H.D., 2009. Sustained turbidity currents and their interaction with debrite-related topography; Labuan Island, offshore NW Borneo, Malaysia. Sedimentary Geology 219, 77-96.
Jobe, Z.R., Lowe, D.R., Uchytil, S.J., 2011. Two fundamentally different types of submarine canyons along the continental margin of Equatorial Guinea. Marine and Petroleum Geology 28, 843-860.
Kane, I.A., Clare, M.A., Miramontes, E., Wogelius, R., Rothwell, J.J., Garreau, P., Pohl, F., 2020. Seafloor microplastic hotspots controlled by deep-sea circulation. Science 368, 1140-1145.
Kneller, B., Dykstra, M., Fairweather, L., Milana, J.P., 2016. Mass-transport and slope accommodation: Implications for turbidite sandstone reservoirs. AAPG Bulletin 100, 213-235.
Krassay, A., Cathro, D., Ryan, D., 2004. A regional tectonostratigraphic framework for the Otway Basin.
Kuleshov, Y., De Hoedt, G., Wright, W., Brewster, A., 2002. Thunderstorm distribution and frequency in Australia. Australian Meteorological Magazine 51, 145.

638 Laberg, J., Vorren, T., Dowdeswell, J., Kenyon, N., Taylor, J., 2000. The Andøya Slide and the Andøya
639 Canyon, north-eastern Norwegian–Greenland Sea. Marine Geology 162, 259-275.
640 Leach, A., Wallace, M., 2001. Cenozoic submarine canyon systems in cool water carbonates from the
641 Otway Basin, Victoria, Australia.
642 Lee, H.J., Locat, J., Desgagnés, P., Parsons, J.D., McAdoo, B.G., Orange, D.L., Puig, P., Wong, F.L., Dartnell,
643 P., Boulanger, E., 2007. Submarine mass movements on continental margins, Continental margin
644 sedimentation: from sediment transport to sequence stratigraphy. Citeseer, pp. 213-274.
645 Li, W., Alves, T.M., Rebesco, M., Sun, J., Li, J., Li, S., Wu, S., 2020. The Baiyun Slide Complex, South China
646 Sea: A modern example of slope instability controlling submarine-channel incision on continental slopes.
647 Marine and Petroleum Geology 114, 104231.
648 Li, W., Alves, T.M., Urlaub, M., Georgiopoulou, A., Klaucke, I., Wynn, R.B., Gross, F., Meyer, M.,
649 Repschläger, J., Berndt, C., 2017. Morphology, age and sediment dynamics of the upper headwall of the
650 Sahara Slide Complex, Northwest Africa: Evidence for a large Late Holocene failure. Marine Geology 393,
651 109-123.
652 Locat, A., Leroueil, S., Bernander, S., Demers, D., Jostad, H.P., Ouehb, L., 2011. Progressive failures in
653 eastern Canadian and Scandinavian sensitive clays. Canadian Geotechnical Journal 48, 1696-1712.
654 Loncke, L., Gaullier, V., Droz, L., Ducassou, E., Migeon, S., Mascle, J., 2009. Multi-scale slope instabilities
655 along the Nile deep-sea fan, Egyptian margin: A general overview. Marine and Petroleum Geology 26,
656 633-646.
657 McAdoo, B., Pratson, L., Orange, D., 2000. Submarine landslide geomorphology, US continental slope.
658 Marine Geology 169, 103-136.
659 McGowran, B., Holdgate, G., Li, Q., Gallagher, S., 2004. Cenozoic stratigraphic succession in southeastern
660 Australia. Australian Journal of Earth Sciences 51, 459-496.
661 Micallef, A., Mountjoy, J.J., Canals, M., Lastras, G., 2012. Deep-seated bedrock landslides and submarine
662 canyon evolution in an active tectonic margin: Cook Strait, New Zealand, Submarine mass movements
663 and their consequences. Springer, pp. 201-212.
664 Middleton, J.F., Bye, J.A., 2007. A review of the shelf-slope circulation along Australia's southern shelves:
665 Cape Leeuwin to Portland. Progress in Oceanography 75, 1-41.
666 Miramontes, E., Eggenhuisen, J.T., Jacinto, R.S., Poneti, G., Pohl, F., Normandeau, A., Campbell, D.C.,
667 Hernández-Molina, F.J., 2020. Channel-levee evolution in combined contour current–turbidity current
668 flows from flume-tank experiments. Geology 48, 353-357.
669 Mitchell, N.C., 2004. Form of submarine erosion from confluences in Atlantic USA continental slope
670 canyons. American Journal of Science 304, 590-611.
671 Moscardelli, L., Wood, L., 2008. New classification system for mass transport complexes in offshore
672 Trinidad. Basin Research 20, 73-98.
673 Moscardelli, L., Wood, L., 2016. Morphometry of mass-transport deposits as a predictive tool. Bulletin
674 128, 47-80.
675 Moscardelli, L., Wood, L., Mann, P., 2006. Mass-transport complexes and associated processes in the
676 offshore area of Trinidad and Venezuela. AAPG bulletin 90, 1059-1088.
677 Normandeau, A., Lajeunesse, P., St-Onge, G., 2015. Submarine canyons and channels in the Lower St.
678 Lawrence Estuary (Eastern Canada): Morphology, classification and recent sediment dynamics.
679 Geomorphology 241, 1-18.
680 Normandeau, A., Lajeunesse, P., St-Onge, G., Bourgault, D., Drouin, S.S.-O., Senneville, S., Belanger, S.,
681 2014. Morphodynamics in sediment-starved inner-shelf submarine canyons (Lower St. Lawrence

682 Estuary, Eastern Canada). Marine Geology 357, 243-255.
683 Nugraha, H.D., Jackson, C.A.-L., Johnson, H.D., Hodgson, D.M., Clare, M., 2019. How erosive are
684 submarine landslides?
685 Obelcz, J., Brothers, D., Chaytor, J., ten Brink, U., Ross, S.W., Brooke, S., 2014. Geomorphic
686 characterization of four shelf-sourced submarine canyons along the US Mid-Atlantic continental margin.
687 Deep Sea Research Part II: Topical Studies in Oceanography 104, 106-119.
688 Ortiz-Karpf, A., Hodgson, D., McCaffrey, W., 2015. The role of mass-transport complexes in controlling
689 channel avulsion and the subsequent sediment dispersal patterns on an active margin: the Magdalena
690 Fan, offshore Colombia. Marine and Petroleum Geology 64, 58-75.
691 Paull, C., Caress, D., Lundsten, E., Gwiazda, R., Anderson, K., McGann, M., Conrad, J., Edwards, B.,
692 Sumner, E., 2013. Anatomy of the La Jolla submarine canyon system; offshore Southern California.
693 Marine Geology 335, 16-34.
694 Perincek, D., Cockshell, C., 1995. The Otway basin: early Cretaceous rifting to Neogene inversion. The
695 APPEA Journal 35, 451-466.
696 Pham, C.K., Ramirez-Llodra, E., Alt, C.H., Amaro, T., Bergmann, M., Canals, M., Company, J.B., Davies, J.,
697 Duineveld, G., Galgani, F., 2014. Marine litter distribution and density in European seas, from the shelves
698 to deep basins. PloS one 9, e95839.
699 Popescu, I., Lericolais, G., Panin, N., Normand, A., Dinu, C., Le Drezen, E., 2004. The Danube submarine
700 canyon (Black Sea): morphology and sedimentary processes. Marine Geology 206, 249-265.
701 Posamentier, H., Erskine, R., Mitchum, R., 1991. Models for submarine-fan deposition within a
702 sequence-stratigraphic framework, Seismic facies and sedimentary processes of submarine fans and
703 turbidite systems. Springer, pp. 127-136.
704 Posamentier, H.W., Martinsen, O.J., 2011. The character and genesis of submarine mass-transport
705 deposits: insights from outcrop and 3D seismic data. Mass-transport deposits in deepwater settings:
706 Society for Sedimentary Geology (SEPM) Special Publication 96, 7-38.
707 Pratson, L.F., Coakley, B.J., 1996. A model for the headward erosion of submarine canyons induced by
708 downslope-eroding sediment flows. Geological Society of America Bulletin 108, 225-234.
709 Pratson, L.F., Ryan, W.B., 1994. Pliocene to recent infilling and subsidence of intraslope basins offshore
710 Louisiana. AAPG bulletin 78, 1483-1506.
711 Puga-Bernabéu, Á., Webster, J.M., Beaman, R.J., Guilbaud, V., 2011. Morphology and controls on the
712 evolution of a mixed carbonate–siliciclastic submarine canyon system, Great Barrier Reef margin, north-
713 eastern Australia. Marine Geology 289, 100-116.
714 Qin, Y., Alves, T.M., Constantine, J., Gamboa, D., 2017. The role of mass wasting in the progressive
715 development of submarine channels (Espirito Santo Basin, SE Brazil). Journal of Sedimentary Research
716 87, 500-516.
717 Rebesco, M., Camerlenghi, A., Volpi, V., Neagu, C., Accettella, D., Lindberg, B., Cova, A., Zgur, F., Party,
718 M., 2007. Interaction of processes and importance of contourites: insights from the detailed
719 morphology of sediment Drift 7, Antarctica. Geological Society, London, Special Publications 276, 95-
720 110.
721 Rebesco, M., Hernández-Molina, F.J., Van Rooij, D., Wåhlin, A., 2014. Contourites and associated
722 sediments controlled by deep-water circulation processes: State-of-the-art and future considerations.
723 Marine Geology 352, 111-154.
724 Ridgway, K., 2007. Seasonal circulation around Tasmania: an interface between eastern and western
725 boundary dynamics. Journal of Geophysical Research: Oceans 112.

Rochford, D., 1986. Seasonal changes in the distribution of Leeuwin Current waters of Southern Australia. Marine and Freshwater Research 37, 1-10.
Sawyer, D.E., 2007. Lateral Variations in Core, Log, and Seismic Attributes of a Mass Transport Complex in the Ursa Region, IODP Expedition 308, Northern Gulf of Mexico.
Sawyer, D.E., DeVore, J.R., 2015. Elevated shear strength of sediments on active margins: Evidence for seismic strengthening. Geophysical Research Letters 42, 10,216-210,221.
Sawyer, D.E., Flemings, P.B., Dugan, B., Germaine, J.T., 2009. Retrogressive failures recorded in mass transport deposits in the Ursa Basin, Northern Gulf of Mexico. Journal of Geophysical Research: Solid Earth 114.
Sequeiros, O.E., Pittaluga, M.B., Frascati, A., Pirmez, C., Masson, D.G., Weaver, P., Crosby, A.R., Lazzaro, G., Botter, G., Rimmer, J.G., 2019. How typhoons trigger turbidity currents in submarine canyons. Scientific reports 9, 1-15.
Shepard, F.P., 1972. Submarine canyons. Earth-Science Reviews 8, 1-12.
Shepard, F.P., Dill, R.F., Dill, R.F., 1966. Submarine canyons and other sea valleys. Rand McNally.
Shepard, F.P., Marshall, N.F., McLoughlin, P.A., 1974. " Internal Waves" Advancing along Submarine Canyons. Science 183, 195-198.
Shipp, R.C., 2004. Physical Characteristics and Impact of Mass Transport Complexes on Deepwater Jetted Conductors and Suction Anchor Piles.
Smith, M.E., Werner, S.H., Buscombe, D., Finnegan, N.J., Sumner, E.J., Mueller, E.R., 2018. Seeking the shore: Evidence for active submarine canyon head incision due to coarse sediment supply and focusing of wave energy. Geophysical Research Letters 45, 12,403-412,413.
Steventon, M.J., Jackson, C.A.-L., Johnson, H.D., Hodgson, D.M., Kelly, S., Omma, J., Gopon, C., Stevenson, C., Fitch, P., 2021. Evolution of a sand-rich submarine channel–lobe system, and the impact of mass-transport and transitional-flow deposits on reservoir heterogeneity: Magnus Field, Northern North Sea. Petroleum Geoscience 27, petgeo2020-2095.
Stow, D., Faugères, J.-C., 2008. Contourite facies and the facies model. Developments in sedimentology 60, 223-256.
Stow, D.A., Mayall, M., 2000. Deep-water sedimentary systems: new models for the 21st century. Marine and Petroleum Geology 17, 125-135.
Su, M., Lin, Z., Wang, C., Kuang, Z., Liang, J., Chen, H., Liu, S., Zhang, B., Luo, K., Huang, S., 2020. Geomorphologic and infilling characteristics of the slope-confined submarine canyons in the Pearl River Mouth Basin, northern South China Sea. Marine Geology 424, 106166.
Tassone, D., Holford, S., Tingay, M., Tuitt, A., Stoker, M., Hillis, R., 2011. Overpressures in the central Otway Basin: the result of rapid Pliocene–Recent sedimentation? The APPEA Journal 51, 439-458.
Totterdell, J., Bradshaw, M., Owen, K., Hashimoto, T., Hall, L., 2014. Petroleum geology inventory of Australia's offshore frontier basins. Geoscience Australia.
Twichell, D.C., Roberts, D.G., 1982. Morphology, distribution, and development of submarine canyons on the United States Atlantic continental slope between Hudson arid Baltimore Canyons. Geology 10, 408-412.
Urgeles, R., Camerlenghi, A., 2013. Submarine landslides of the Mediterranean Sea: Trigger mechanisms, dynamics, and frequency-magnitude distribution. Journal of Geophysical Research: Earth Surface 118, 2600-2618.
Vail, P., 1977. Seismic stratigraphy and global changes of sea level. Bull. Am. Assoc. Petrol. Geol., Mem.

26, 49-212.
Warratz, G., Schwenk, T., Voigt, I., Bozzano, G., Henrich, R., Violante, R., Lantzsch, H., 2019. Interaction of a deep-sea current with a blind submarine canyon (Mar del Plata Canyon, Argentina). Marine Geology 417, 106002.
Watson, S.J., Mountjoy, J.J., Crutchley, G.J., 2020. Tectonic and geomorphic controls on the distribution of submarine landslides across active and passive margins, eastern New Zealand. Geological Society, London, Special Publications 500, 477-494.
Weimer, P., Slatt, R.M., 2004. Petroleum systems of deepwater settings. Society of Exploration Geophysicists and European Association of ….
Willcox, J., Stagg, H., 1990. Australia's southern margin: a product of oblique extension. Tectonophysics 173, 269-281.
Williams, S.C., 2016. News Feature: Skimming the surface of underwater landslides. Proceedings of the National Academy of Sciences 113, 1675-1678.
Wu, N., Jackson, C.A.L., Johnson, H.D., Hodgson, D.M., Clare, M.A., Nugraha, H.D., Li, W., 2021. The formation and implications of giant blocks and fluid escape structures in submarine lateral spreads. Basin Research.
Xu, J., Swarzenski, P.W., Noble, M., Li, A.-C., 2010. Event-driven sediment flux in Hueneme and Mugu submarine canyons, southern California. Marine Geology 269, 74-88.
Zhong, G., Cartigny, M.J., Kuang, Z., Wang, L., 2015. Cyclic steps along the South Taiwan Shoal and West Penghu submarine canyons on the northeastern continental slope of the South China Sea. Bulletin 127, 804-824.
Zhong, G., Peng, X., 2021. Transport and accumulation of plastic litter in submarine canyons—The role of gravity flows. Geology 49, 581-586.
Zhu, M., Graham, S., Pang, X., McHargue, T., 2010. Characteristics of migrating submarine canyons from the middle Miocene to present: Implications for paleoceanographic circulation, northern South China Sea. Marine and Petroleum Geology 27, 307-319.

Figure 1

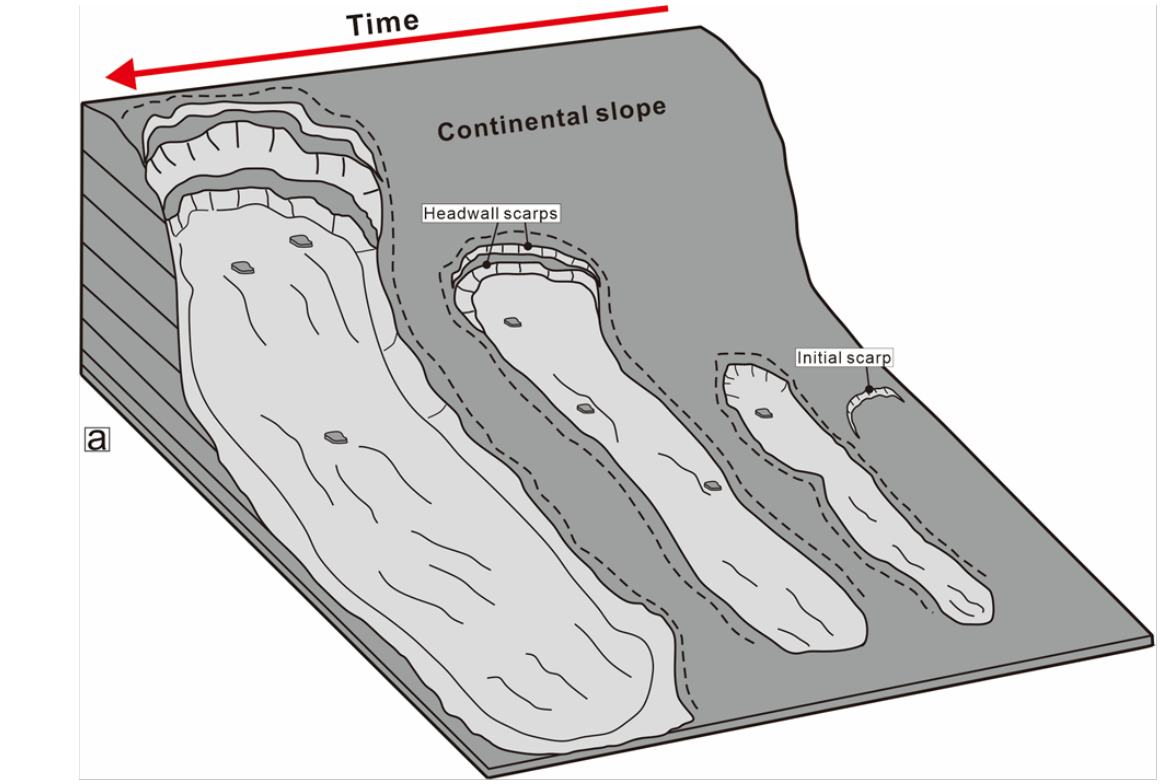
Time
Continental slope
Headwall scarps
Initial scarp
a

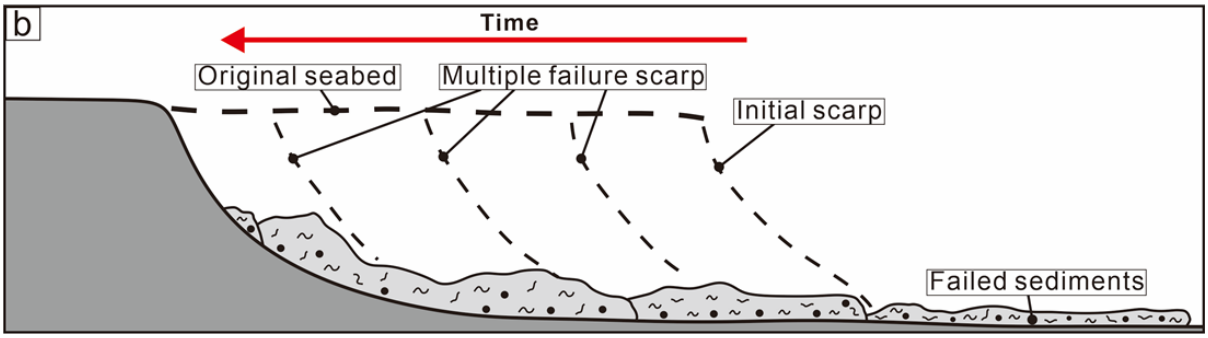
b
Time
Original seabed
Multiple failure scarp
Initial scarp
Failed sediments

Figure 2

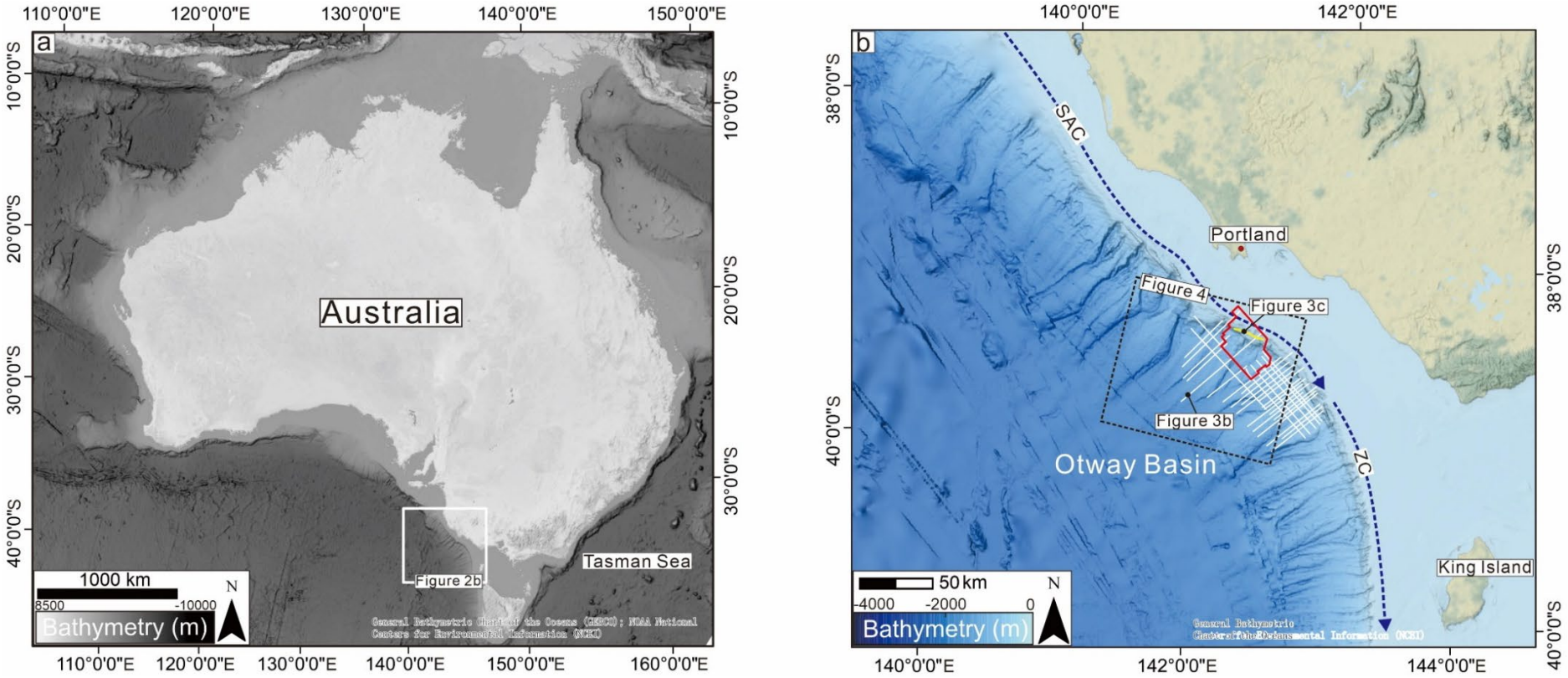
a
110°0'0"E
120°0'0"E
130°0'0"E
140°0'0"E
150°0'0"E
160°0'0"E
10°0'0"S
20°0'0"S
30°0'0"S
40°0'0"S
Australia
Tasman Sea
Figure 2b
1000 km
8500
-10000
N
Bathymetry (m)
b
140°0'0"E
142°0'0"E
144°0'0"E
38°0'0"S
40°0'0"S
SAC
Portland
Figure 4
Figure 3c
Figure 3b
Otway Basin
ZC
King Island
50 km
-4000
-2000
0
N
Bathymetry (m)

Figure 3

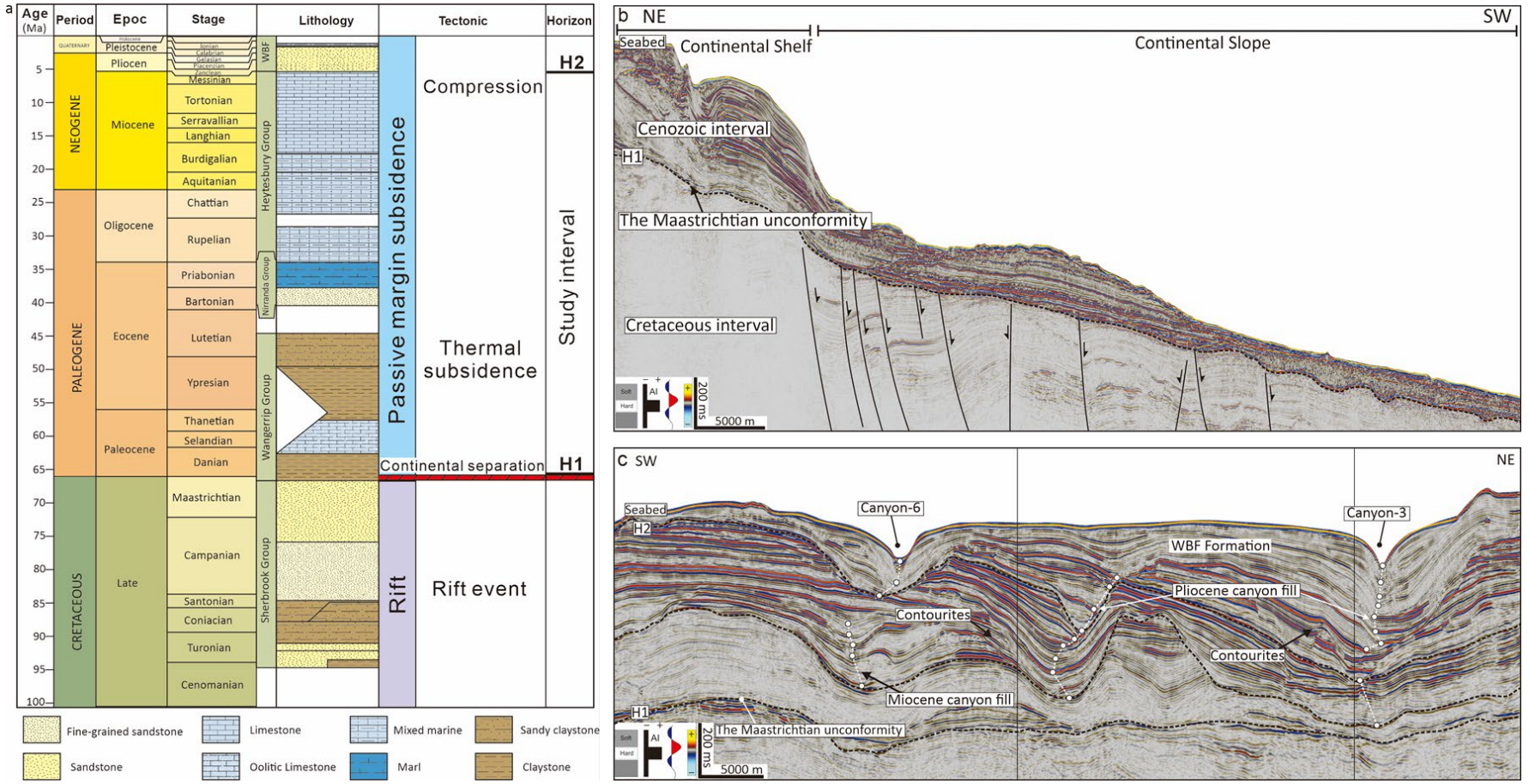
a
Age (Ma)
Period
Epoc
Stage
Lithology
Tectonic
Horizon
NEOGENE
PALEOGENE
CRETACEOUS
Pleistocene
Pliocen
Miocene
Oligocene
Eocene
Paleocene
Late
Messinian
Tortonian
Serravallian
Langhian
Burdigalian
Aquitanian
Chattian
Rupelian
Priabonian
Bartonian
Lutetian
Ypresian
Thanetian
Selandian
Danian
Maastrichtian
Campanian
Santonian
Coniacian
Turonian
Cenomanian
WBF
Heytesbury Group
Nirranda Group
Wangerrip Group
Sherbrook Group
Passive margin subsidence
Rift
Compression
Thermal subsidence
Rift event
Continental separation
H2
H1
Study interval
Fine-grained sandstone
Sandstone
Limestone
Oolitic Limestone
Mixed marine
Marl
Sandy claystone
Claystone
b NE
SW
Seabed
Continental Shelf
Continental Slope
Cenozoic interval
H1
The Maastrichtian unconformity
Cretaceous interval
200 ms
5000 m
c SW
NE
Seabed
H2
Canyon-6
Canyon-3
WBF Formation
Pliocene canyon fill
Contourites
Contourites
Miocene canyon fill
H1
The Maastrichtian unconformity
200 ms
5000 m

Figure 4

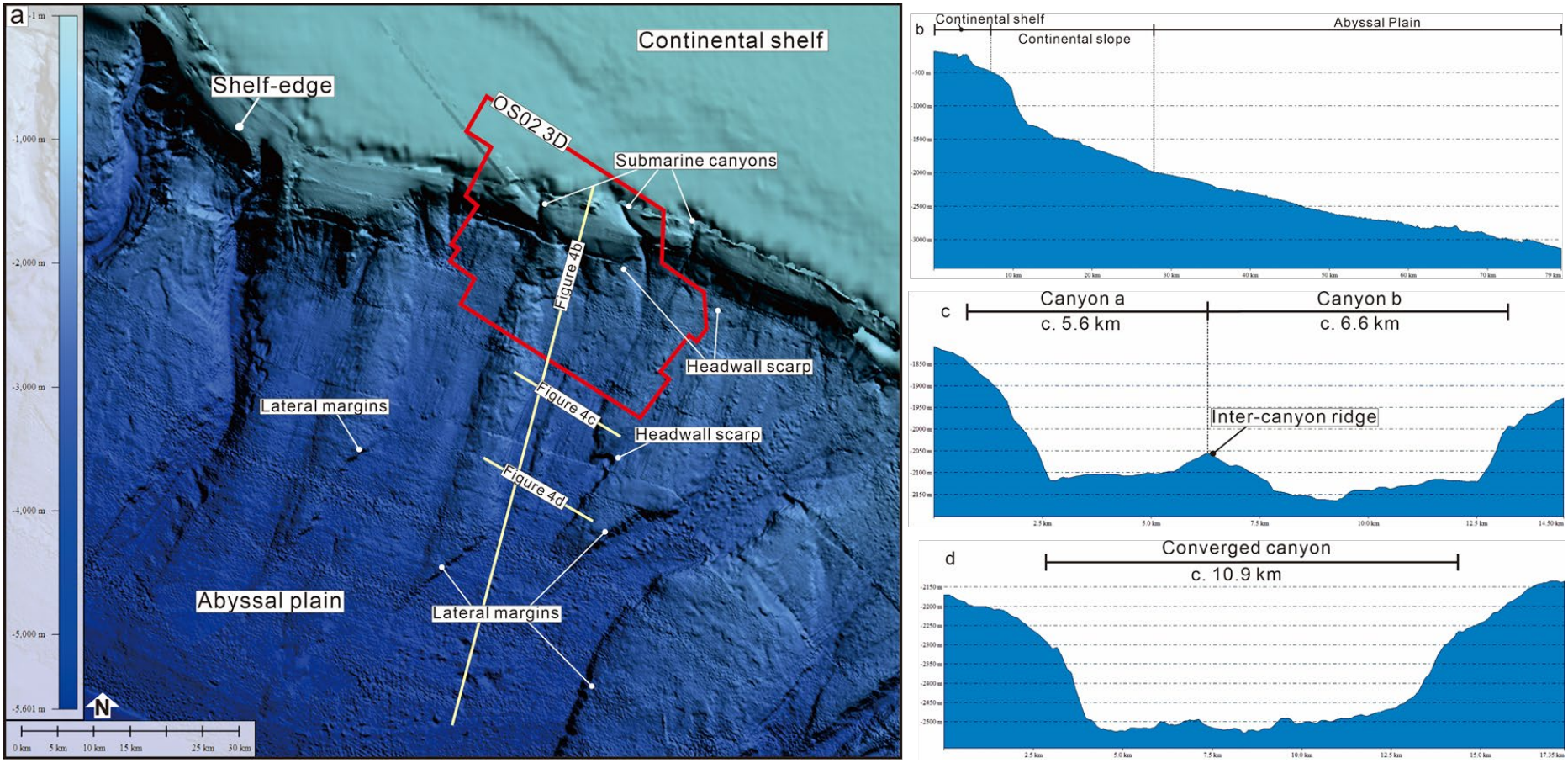
a
Continental shelf
Shelf-edge
OS02 3D
Submarine canyons
Figure 4b
Figure 4c
Figure 4d
Headwall scarp
Lateral margins
Headwall scarp
Abyssal plain
Lateral margins
N
b
Continental shelf
Continental slope
Abyssal Plain
c
Canyon a
c. 5.6 km
Canyon b
c. 6.6 km
Inter-canyon ridge
d
Converged canyon
c. 10.9 km

Figure 5

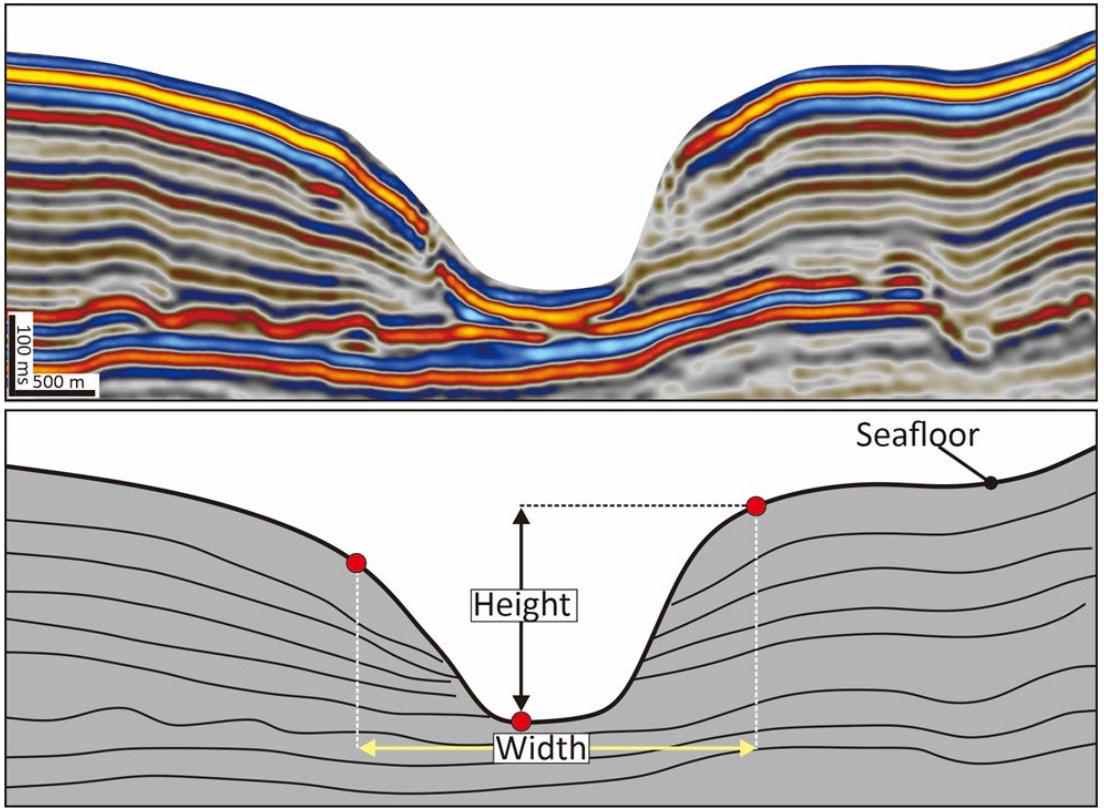

Figure 6

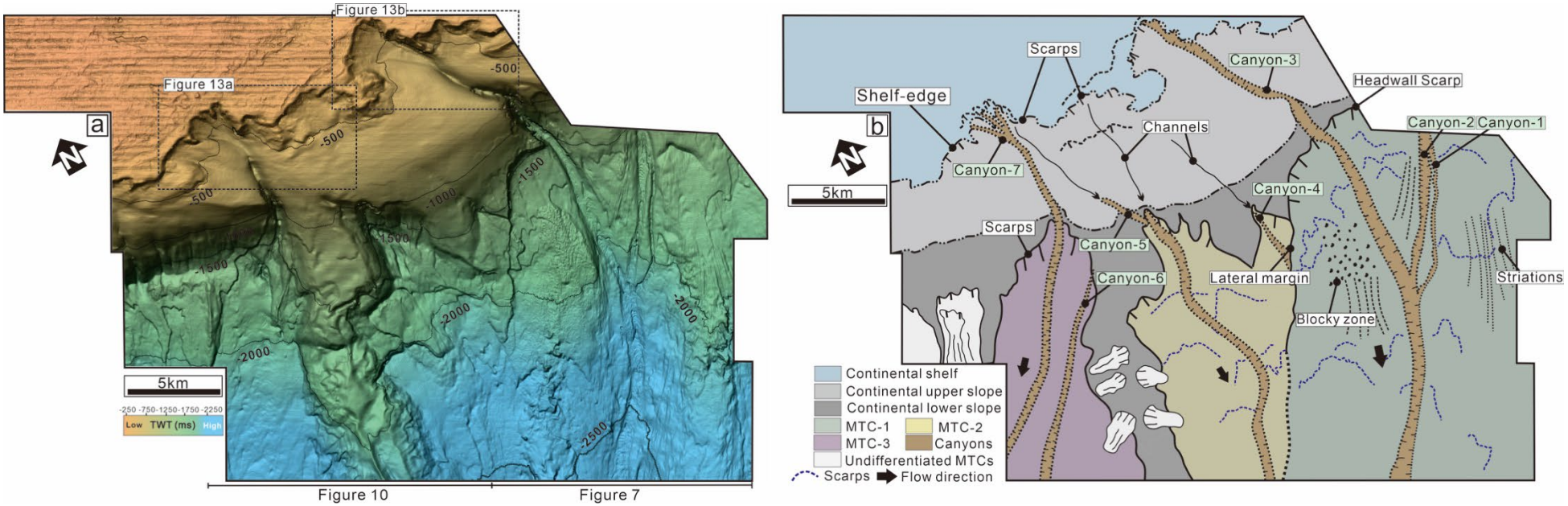
Figure 13b
Figure 13a
a
N
-500
-1000
-1500
-2000
-2500
5km
-250 -750-1250-1750 -2250
Low TWT (ms) High
Figure 10
Figure 7
b
N
5km
Shelf-edge
Scarps
Canyon-3
Headwall Scarp
Channels
Canyon-2
Canyon-1
Canyon-7
Canyon-4
Scarps
Canyon-5
Canyon-6
Lateral margin
Striations
Blocky zone
Continental shelf
Continental upper slope
Continental lower slope
MTC-1
MTC-2
MTC-3
Canyons
Undifferentiated MTCs
Scarps
Flow direction

Figure 7

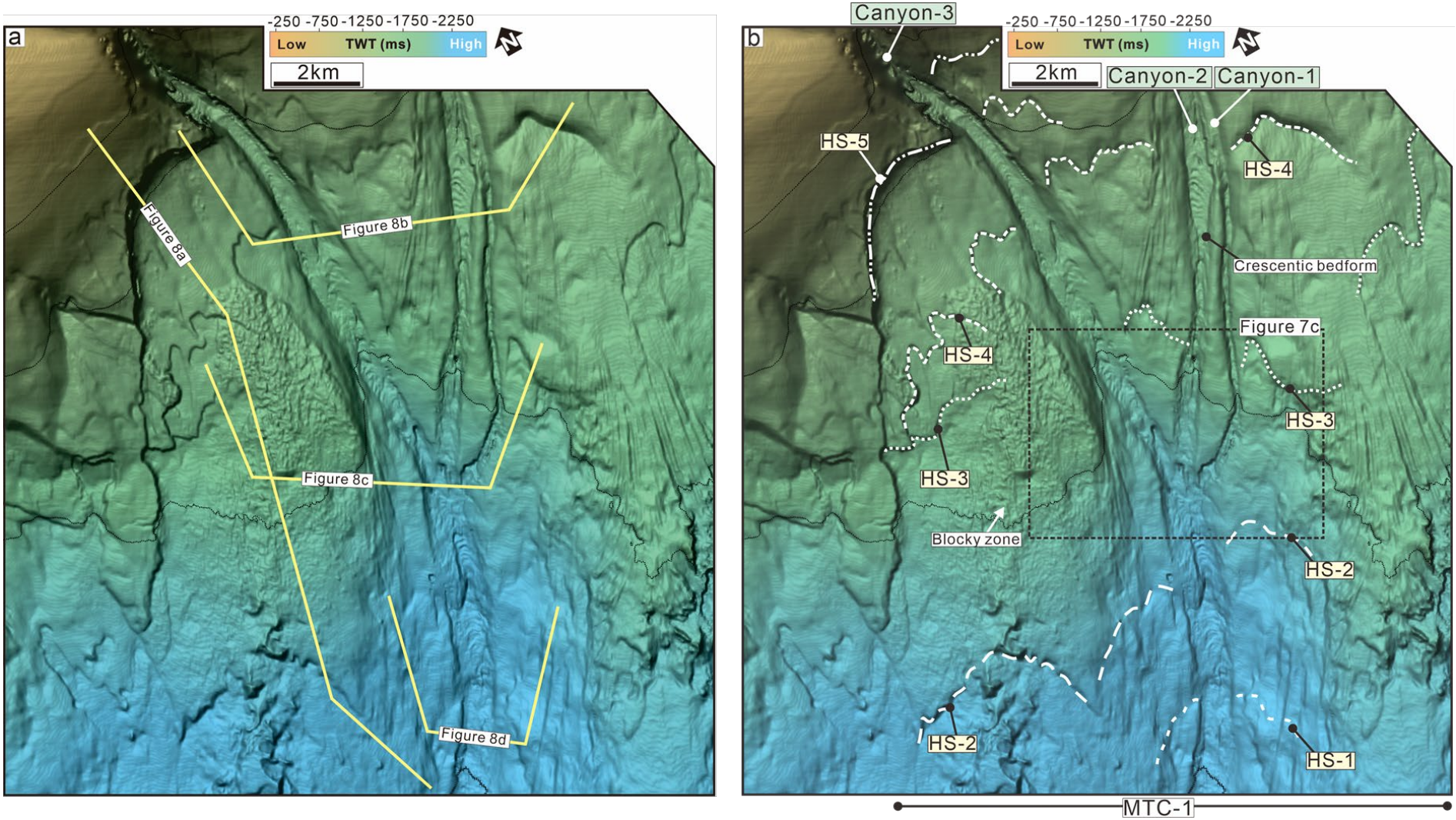
a
-250 -750 -1250 -1750 -2250
Low TWT (ms) High
2km
Figure 8a
Figure 8b
Figure 8c
Figure 8d
b
Canyon-3
Canyon-2
Canyon-1
HS-5
HS-4
Crescentic bedform
Figure 7c
HS-4
HS-3
HS-3
Blocky zone
HS-2
HS-2
HS-1
MTC-1

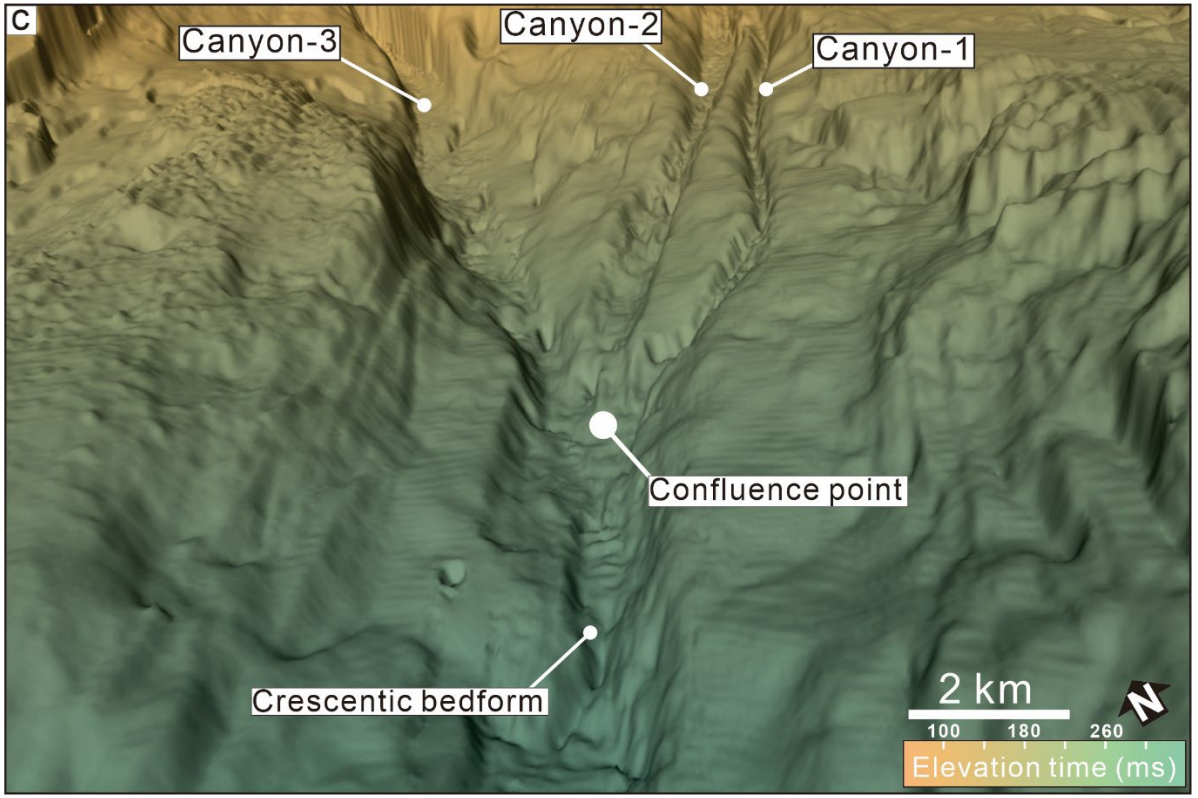
c
Canyon-3
Canyon-2
Canyon-1
Confluence point
Crescentic bedform
2 km
N
100
180
260
Elevation time (ms)

Figure 8

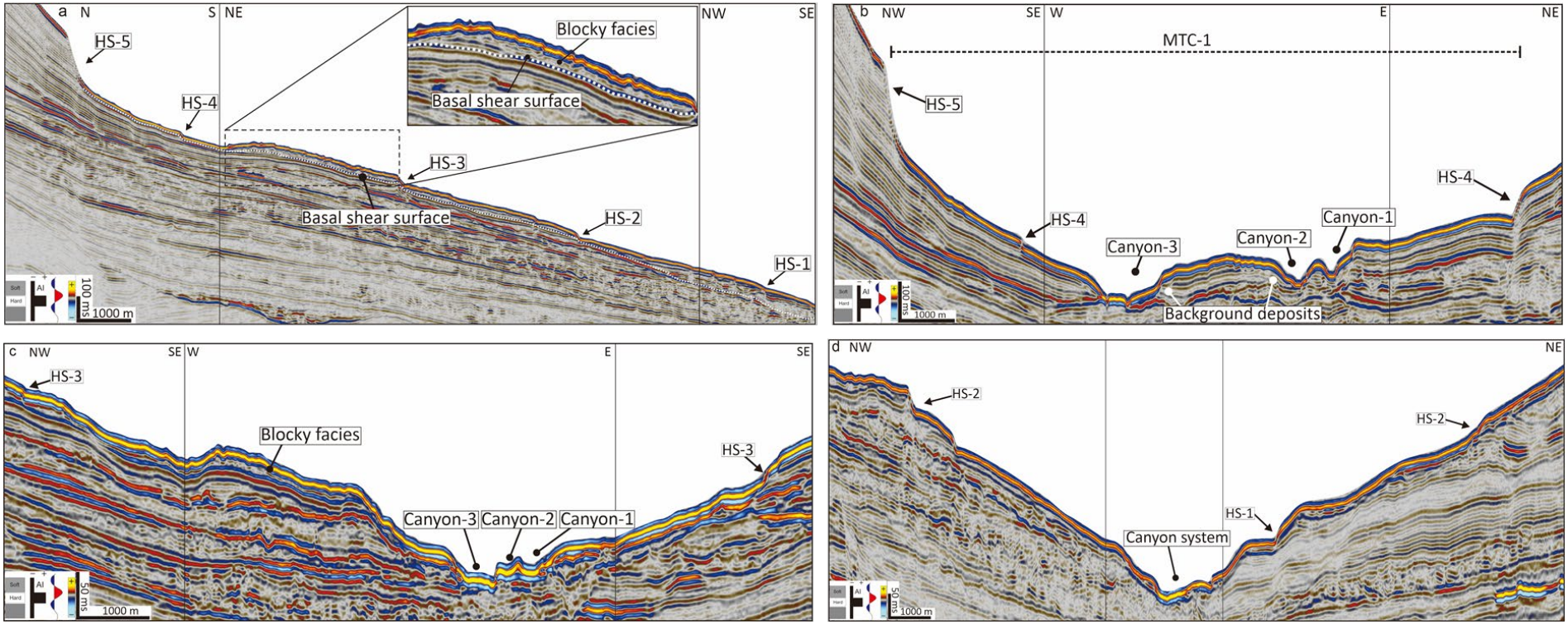
a N S NE NW SE
HS-5
HS-4
Blocky facies
Basal shear surface
HS-3
Basal shear surface
HS-2
HS-1
100 ms
1000 m
b NW SE W E NE
MTC-1
HS-5
HS-4
Canyon-3
Canyon-2
Canyon-1
HS-4
Background deposits
100 ms
1000 m
c NW SE W E SE
HS-3
Blocky facies
HS-3
Canyon-3
Canyon-2
Canyon-1
50 ms
1000 m
d NW NE
HS-2
HS-2
HS-1
Canyon system
50 ms
1000 m

Figure 9

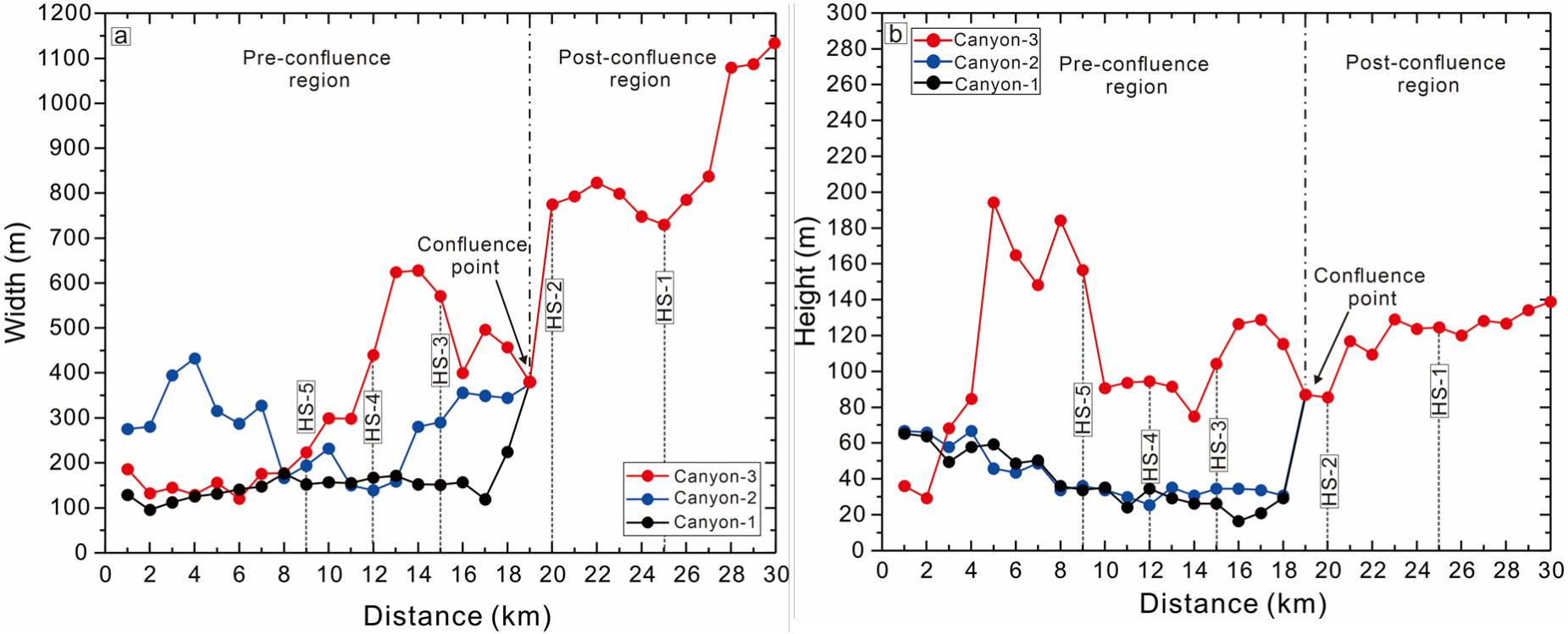
a
Pre-confluence region
Post-confluence region
Confluence point
HS-5
HS-4
HS-3
HS-2
HS-1
Canyon-3
Canyon-2
Canyon-1
Width (m)
Distance (km)
b
Pre-confluence region
Post-confluence region
Confluence point
HS-5
HS-4
HS-3
HS-2
HS-1
Canyon-3
Canyon-2
Canyon-1
Height (m)
Distance (km)

Figure 10

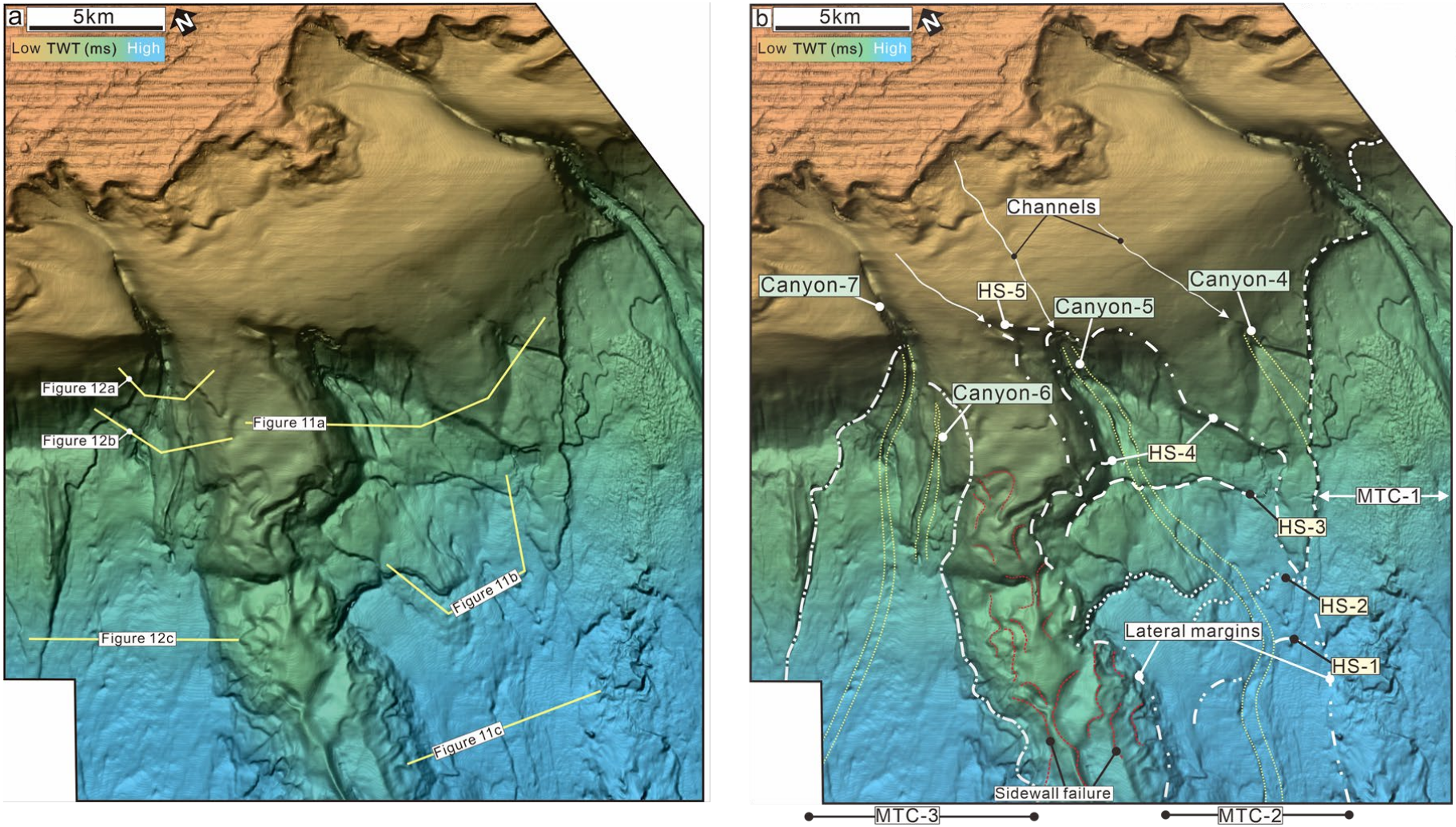
a
5km
N
Low TWT (ms) High
Figure 12a
Figure 12b
Figure 11a
Figure 11b
Figure 12c
Figure 11c
b
5km
N
Low TWT (ms) High
Channels
Canyon-7
HS-5
Canyon-5
Canyon-4
Canyon-6
HS-4
MTC-1
HS-3
HS-2
Lateral margins
HS-1
Sidewall failure
MTC-3
MTC-2

Figure 11

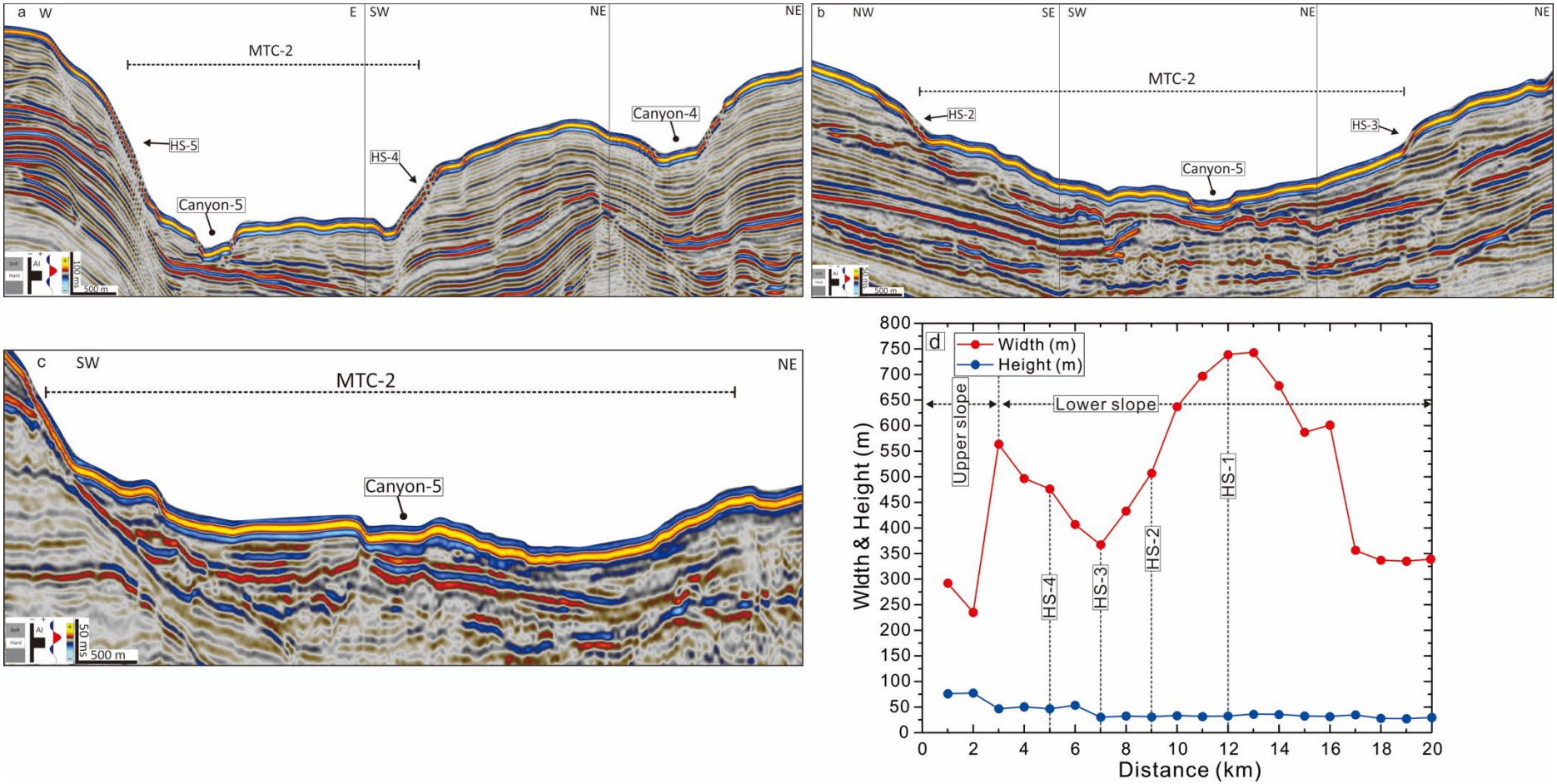
a
W
E
SW
NE
NE
MTC-2
HS-5
HS-4
Canyon-5
Canyon-4
100 ms
500 m
b
NW
SE
SW
NE
NE
MTC-2
HS-2
HS-3
Canyon-5
50 ms
500 m
c
SW
NE
MTC-2
Canyon-5
50 ms
500 m
d
Width (m)
Height (m)
Upper slope
Lower slope
HS-1
HS-2
HS-3
HS-4
Width & Height (m)
Distance (km)
0
50
100
150
200
250
300
350
400
450
500
550
600
650
700
750
800
0
2
4
6
8
10
12
14
16
18
20

Figure 12

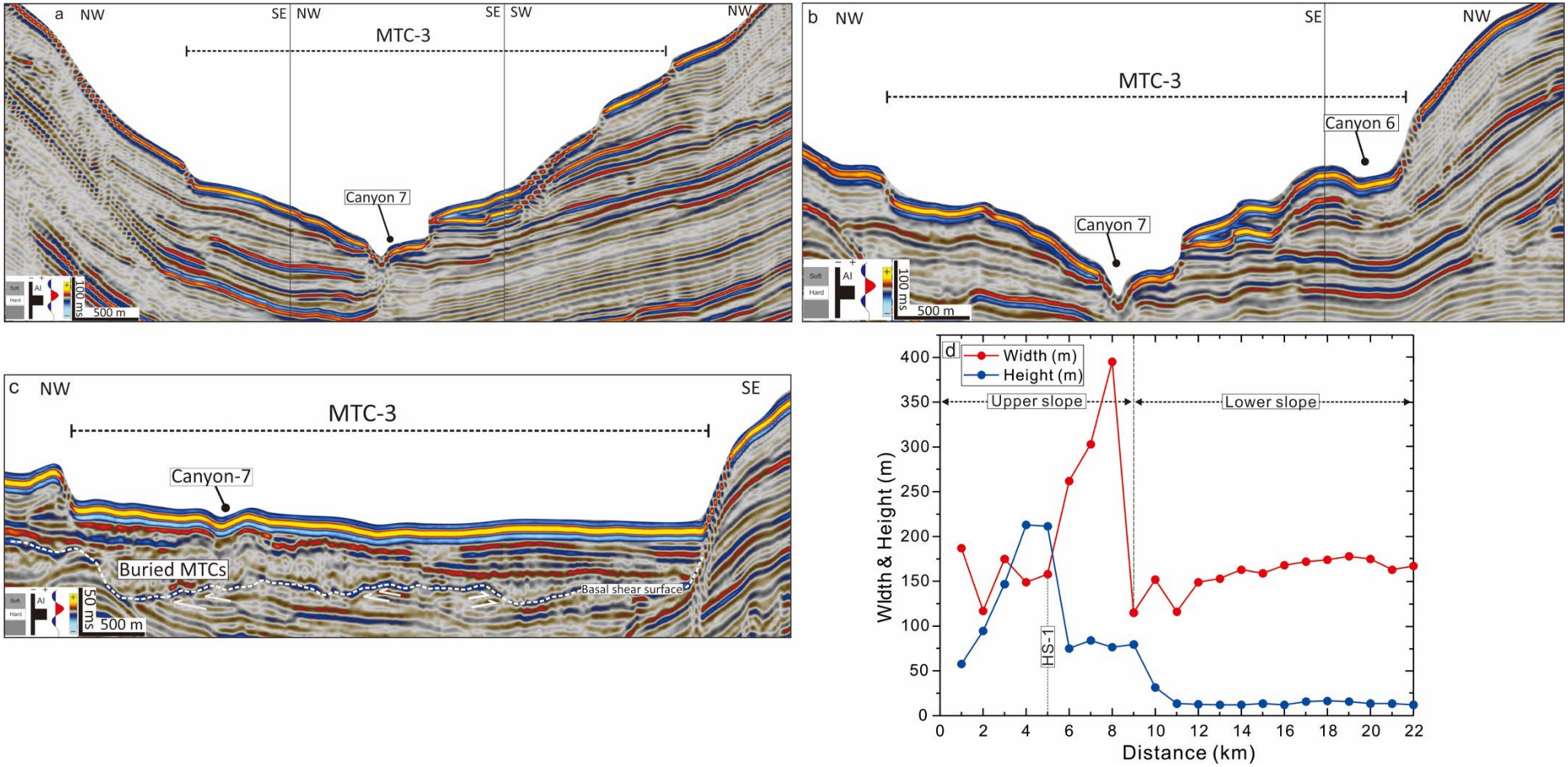
a
NW
SE
NW
SE
SW
NW
MTC-3
Canyon 7
100 ms
500 m
b
NW
SE
NW
MTC-3
Canyon 6
Canyon 7
100 ms
500 m
c
NW
SE
MTC-3
Canyon-7
Buried MTCs
Basal shear surface
50 ms
500 m
d
Width (m)
Height (m)
Upper slope
Lower slope
HS-1
Width & Height (m)
Distance (km)
0
50
100
150
200
250
300
350
400
0
2
4
6
8
10
12
14
16
18
20
22

Figure 13

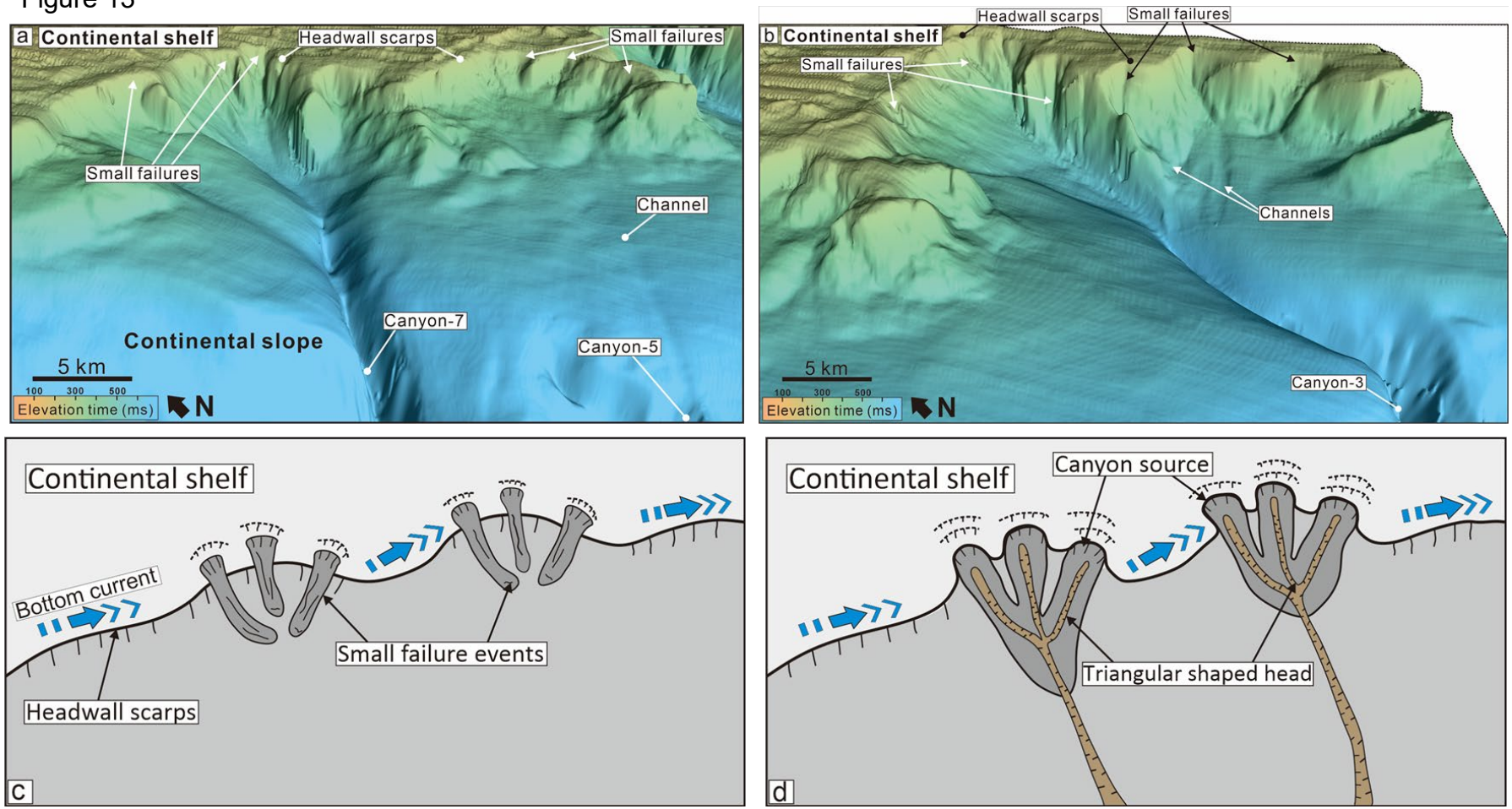
a Continental shelf
Headwall scarps
Small failures
Small failures
Channel
Continental slope
Canyon-7
Canyon-5
5 km
100 300 500
Elevation time (ms)
N
b Continental shelf
Headwall scarps
Small failures
Small failures
Channels
Canyon-3
5 km
100 300 500
Elevation time (ms)
N
Continental shelf
Bottom current
Small failure events
Headwall scarps
c
Continental shelf
Canyon source
Triangular shaped head
d

Figure 14

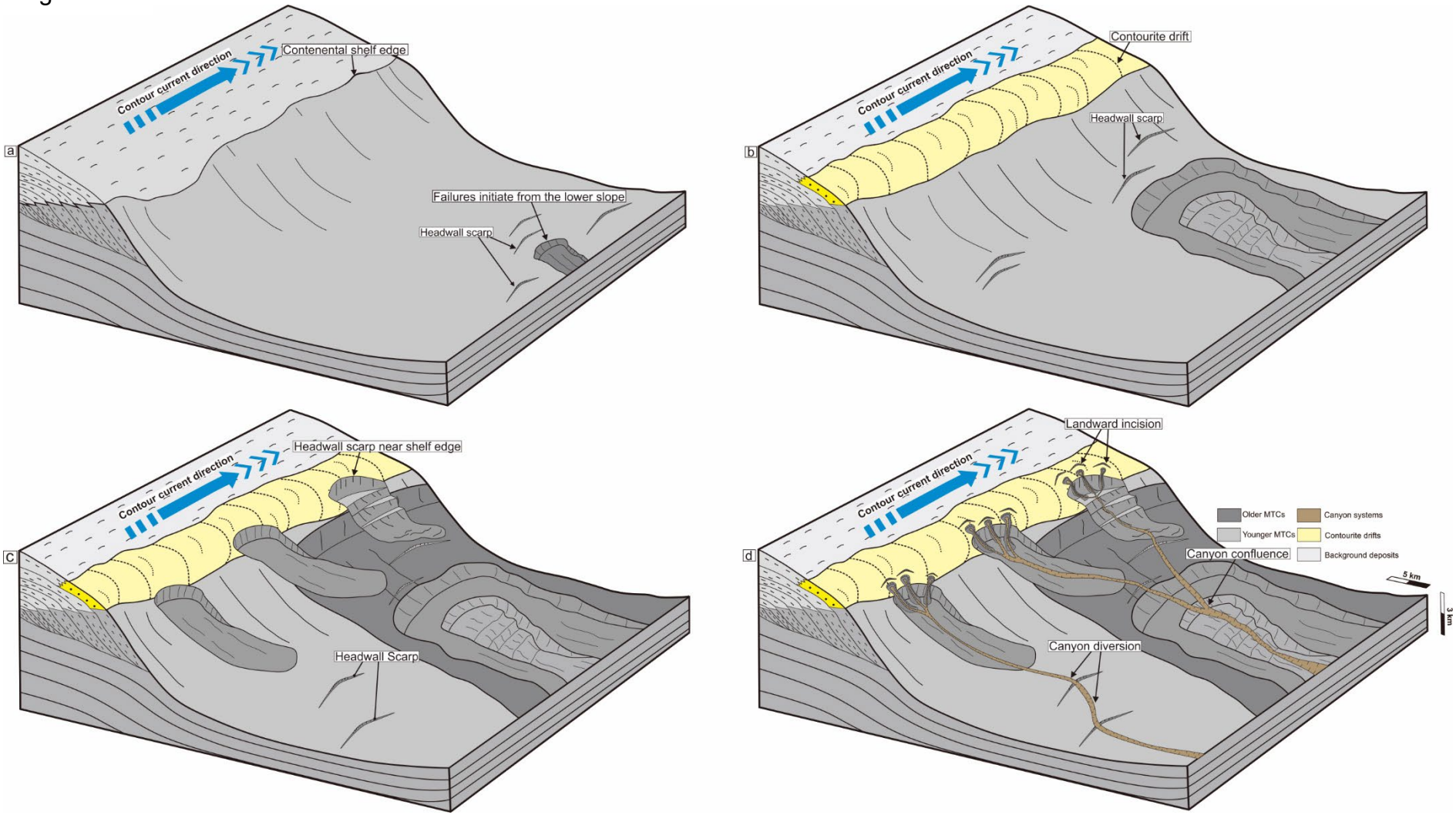
a
Contour current direction
Contenental shelf edge
Failures initiate from the lower slope
Headwall scarp
b
Contour current direction
Contourite drift
Headwall scarp
c
Contour current direction
Headwall scarp near shelf edge
Headwall Scarp
d
Contour current direction
Landward incision
Older MTCs
Younger MTCs
Canyon systems
Contourite drifts
Background deposits
Canyon confluence
Canyon diversion
5 km
3 km

Classification	MTC	Headwall scarps	Canyons	Influences imposed on canyons
Type-1	MTC-1	HS-1 to HS-5	Canyons 1-3	Canyon confluence, widening and deepening
	MTC-2	HS-1 to HS-5	Canyon-5	Canyon transport direction diversion
Type-2	MTC-3	None	Canyons 6-7	No canyon confluence nor diversion

Table 1. Classification of MTCs. Note that MTCs are the abbreviation of mass-transport complexes, and HS equals headwall scarps.